Atlantic Geoscience
Journal of the Atlantic Geoscience Society

Further evidence for the East Coast fault system and faults associated with the Summerville restraining bend and their possible relationship to the 1886 Charleston, South Carolina, earthquake, USA

Autre preuve de l'existence du système de failles de la Côte est et des failles associées à l'inflexion de restriction de Summerville ainsi que de leur lien possible avec le séisme survenu à Charleston, en Caroline du Sud, aux États-Unis

Ronald T. Marple and James D. Hurd Jr.

Volume 58, 2022

URI: https://id.erudit.org/iderudit/1089924ar
DOI: https://doi.org/10.4138/atlgeo.2022.004

See table of contents

Publisher(s)

Atlantic Geoscience Society

ISSN

2564-2987 (digital)

Explore this journal

Cite this article

Marple, R. & Hurd Jr., J. (2022). Further evidence for the East Coast fault system and faults associated with the Summerville restraining bend and their possible relationship to the 1886 Charleston, South Carolina, earthquake, USA. *Atlantic Geoscience*, *58*, 99–129. https://doi.org/10.4138/atlgeo.2022.004

Article abstract

The integration of aeromagnetic, LiDAR, and previously acquired seismic-reflection data and surficial geologic maps supports the existence of the East Coast fault system (and faults associated with its 12º Summerville restraining bend beneath the South Carolina Coastal Plain. Aeromagnetic data revealed a 10- to 15-km-wide zone of subtle, 22- to 35-km-long linear magnetic anomalies trending ~N10°E across the southern meizoseismal area of the 1886 Charleston earthquake that we postulate are associated with Cenozoic low-displacement brittle faults in the crystalline basement west of Charleston. We hypothesize that lineaments ML4 and ML5 represent the principal displacement zone along the southern end of the ECFS because they coincide with steeply dipping, west-side-up buried faults interpreted from previously acquired seismic-reflection profiles and a ~320-m dextral offset in the Brownsville Pleistocene beach ridge deposit. The alignment of the NNE-SSW-oriented Edisto dome, uplift along releveling line 9, gently upwarped longitudinal profiles along the Caw Caw and Horse Savanna swamps, local incision along the Ashley River, and exposures of the early Oligocene Ashley Formation near the incised part of the Ashley River support Quaternary uplift along the southern ECFS. The 12º change in trend formed by lineaments ML4 and ML5 supports the existence of the Summerville restraining bend in the ECFS, east of which are numerous ENE-WSW- to NW-SE-oriented LiDAR lineaments that we postulate are surface expressions of faults that formed to compensate for the increased compression produced by dextral motion along the bend. Sinistral displacement along one of these proposed faults associated with the ~40-km-long, east-west-oriented Deer Park lineament may have produced the main shock of the 1886 Charleston earthquake.

Further evidence for the East Coast fault system and faults associated with the Summerville restraining bend and their possible relationship to the 1886 Charleston earthquake, South Carolina, USA

Ronald T. Marple [1] and James D. Hurd, Jr.[2]

1. 215 Cattail Circle, Harker Heights, Texas 76548, USA
2. Department of Natural Resources and the Environment, The University of Connecticut U-87, 1376 Storrs Road, Storrs, Connecticut 06269-4087, USA
Corresponding author <ronmarple@verizon.net>

Date received: 31 January 2022 ¶ Date accepted:28 April 2022

ABSTRACT

The integration of aeromagnetic, LiDAR, and previously acquired seismic-reflection data and surficial geologic maps supports the existence of the East Coast fault system (ECFS) and faults associated with its 12° Summerville restraining bend beneath the South Carolina Coastal Plain. Aeromagnetic data revealed a 10- to 15-km-wide zone of subtle, 22- to 35-km-long linear magnetic anomalies trending ~N10°E across the southern meizoseismal area of the 1886 Charleston earthquake that we postulate are associated with Cenozoic low-displacement brittle faults in the crystalline basement west of Charleston. We hypothesize that lineaments ML4 and ML5 represent the principal displacement zone along the southern end of the ECFS because they coincide with steeply dipping, west-side-up buried faults interpreted from previously acquired seismic-reflection profiles and dextral offset of ~320 m in the Brownsville Pleistocene beach ridge deposit. The alignment of the NNE-SSW-oriented Edisto dome, uplift along releveling line 9, gently upwarped longitudinal profiles along the Caw Caw and Horse Savanna swamps, local incision along the Ashley River, and exposures of the early Oligocene Ashley Formation near the incised part of the Ashley River support Quaternary uplift along the southern ECFS. The 12° change in trend formed by lineaments ML4 and ML5 supports the existence of the Summerville restraining bend along the ECFS, east of which are numerous ENE-WSW- to NW-SE-oriented LiDAR lineaments that we postulate are surface expressions of faults that formed to compensate for the increased compression produced by dextral motion along the bend. Sinistral displacement along one of these proposed faults associated with the ~40-km-long, east-west-oriented Deer Park lineament may have produced the main shock of the 1886 Charleston earthquake.

RÉSUMÉ

L'intégration de données aéromagnétiques, de données lidar et de données de réflexion sismique récemment obtenues ainsi que de cartes géologiques de surface appuie l'existence du système de failles de la Côte est (SFCE) et des failles associées à son inflexion de restriction de 12 degrés de Summerville au-dessous de la plaine côtière de la Caroline du Sud. Les données aéromagnétiques ont révélé une zone de 10 à 15 kilomètres de largeur d'anomalies magnétiques linéaires subtiles sur une longueur de 22 à 35 kilomètres, orientées approximativement vers le nord à 10 degrés est à travers l'aire pléistoséiste méridionale du séisme de Charleston de 1886 qui, postulons-nous, sont associés à des failles cassantes de faible déplacement, cénozoïques, dans le socle cristallin à l'ouest de Charleston. Nous supposons que les linéaments ML4 et ML5 représentent la principale zone de déplacement le long de l'extrémité méridionale du SFCE parce qu'ils coïncident avec des failles enfouies dont le toit est à l'ouest et qui s'inclinent profondément, interprétées à partir de profils de réflexion sismique précédemment obtenus et du mouvement dextre d'environ 320 mètres dans le dépôt de la levée de plage du Pléistocène de Brownsville. L'alignement du dôme Edisto orienté du nord-nord-est au sud-sud-ouest, le soulèvement le long de la ligne du levé d'appoint 9, les profils longitudinaux doucement bombés le long des marécages Caw Caw et Horse Savanna, l'incision locale longeant la rivière Ashley et les affleurements de la Formation de l'Oligocène précoce d'Ashley près de la partie enfoncée de la rivière Ashley appuient l'hypothèse d'un soulèvement quaternaire le long du SFCE méridional. La variation de 12 degrés de l'orientation créée par les linéaments ML4 et ML5 appuie l'existence de l'inflexion de restriction de Summerville dans le SFCE, à l'est des nombreux linéaments lidar orientés de l'est-

doi:10.4138/atlgeo.2022.004

nord-est/ouest-sud-ouest au nord-ouest/sud-est que nous supposons des expressions en surface de failles qui se sont formées pour compenser la compression accrue produite par le mouvement dextre le long de l'inflexion. Le mouvement senestre le long des failles proposées associé au linéament d'une quarantaine de kilomètres de longueur orienté d'est en ouest de Deer Park pourrait avoir produit la principale secousse du séisme de Charleston de 1886.

[*Traduit par la redaction*]

INTRODUCTION

The main shock of the August 31, 1886 earthquake occurred northwest of Charleston, South Carolina, near Woodstock at ~9:51 PM, followed 8–10 minutes later by a smaller earthquake west of Rantowles to the south (Dutton 1889, pp. 215 and 273) (Fig. 1). Moment magnitude, M_w, estimates of the main shock range from 6.9 (Bakun and Hopper 2004) to 7.3 (Johnston 1996). Based on Wells and Coppersmith's (1994) study of earthquake magnitude versus fault rupture length, the fault rupture that produced the main shock was likely at least 25 km long.

Contemporary reports suggest that two epicenters were associated with the Charleston earthquake (Woodstock and Rantowles) (Dutton 1889) and possibly a third one near Middleton Place (McKinley 1887) (Fig. 1). The location of the Rantowles epicenter is less certain because of fewer anthropogenic structures and swampier conditions in the southern meizoseismal area (Dutton 1889). The complex shape of Earle Sloan's isoseismal contours (Dutton 1889, plate XXVII) (Fig. 1) and the 8–10 minute separation between the two earthquakes suggest that at least two faults ruptured August 31, 1886: one trending east-west north of the Ashley River and the other trending NNE-SSW in the southern meizoseismal area. The right-lateral displacement of the Charleston & Savannah Railroad near Rantowles (Dutton 1889, plate XXV) (Fig. 2) suggests that the second earthquake west of Rantowles was produced by dextral strike-slip displacement on a NNE-SSW-oriented fault.

Despite numerous investigations of the meizoseismal area (e.g., Rankin 1977; Gohn 1983), the location and orientation of the causative faults have remained elusive for several reasons. First, the modern seismicity in the area has been sparse and clustered (e.g., Chapman *et al.* 2016), rather than along well-defined trends. Furthermore, little seismicity has been recorded in the areas of greatest intensity near Woodstock and Rantowles (Fig. 2). Thus, the Middleton Place-Summerville seismic zone (MPSSZ) may not accurately reflect the locations of the faults that ruptured August 31, 1886. Second, fault plane solutions from the MPSSZ show a wide variety of fault types and orientations (Shedlock 1988; Madabhushi and Talwani 1993; Chapman *et al.* 2016) that are from displacements along several faults with different orientations. Third, faulting beneath the 700- to 1100-m-thick, southeast-dipping wedge of Cretaceous and Cenozoic unlithified sediments and weakly lithified to indurated sedimentary rocks beneath the Charleston region (Gohn 1988) would likely fold rather than fracture the overlying strata (Stein and Yeats 1989). Fourth, the swampy, densely forested area throughout much of the meizoseismal area makes it difficult to identify surface evidence of faulting. Fifth, the humid climate, easily eroded surface sediments, and the rapid urbanization of the Charleston region in modern time have erased much of the evidence of ground rupture that may have once existed. Finally, low Cenozoic fault slip rates in the eastern United States (Prowell 1988, 0.3–1.5 m/myr) result in small cumulative displacements, thus making it difficult to identify Cenozoic faults in the landscape and on regional aeromagnetic and gravity maps.

Because of these factors, numerous hypotheses have been presented to explain the 1886 Charleston earthquake and MPSSZ. Seeber and Armbruster (1981), for example, proposed that backslip on the Appalachian décollement caused the main shock. Talwani (1982) postulated that the Charleston earthquake and MPSSZ are from stresses produced by the intersection of the NNE-SSW-oriented Woodstock fault and the NW-SE-oriented Ashley River fault. Behrendt (1983) proposed that displacement on a NE-SW-oriented listric fault along the southeastern edge of the Triassic Jedburg basin near Summerville may have caused the Charleston earthquake. Using a digital elevation model and river morphology, Rhea (1989) interpreted a topographically high area in the northwestern part of the Charleston region that she postulated is from uplift, although she did not

Figure 1. (next page) Summary map showing structural domes (bold contours), buried faults interpreted from seismic-reflection profiles (solid triangles, U on upthrown side), and linear magnetic anomalies ML1–ML5 (green lines). Abbreviations of faults (black lines), LiDAR lineaments (blue lines), and scarps are shown in Tables 1 and 2. The thick red parallel lines represent the interpreted uplift along the ZRA and ECFS. Red dots are epicenters of small modern earthquakes east of Adams Run (U.S. Geological Survey 2021). The incised part of the Ashley River is highlighted with thick red contour. Red contours labeled 1–3 are LiDAR-derived elevation profiles along the Caw Caw and Horse Savanna swamps and along the Ashley River valley and Cypress Swamp (uplifted parts are dashed). Orange patterns along the lower Ashley River valley are Pleistocene fluvial terraces from Marple and Hurd (2020). Lines labeled 4–8 are elevation profiles across the Ashley River valley and Cypress Swamp. The dashed contour is the outer isoseismal contour of Sloan (Dutton 1889). Index map in the upper left shows the location of the study area with the Modified Mercalli Intensity contours of the 1886 Charleston earthquake from Bollinger (1977) overlain.

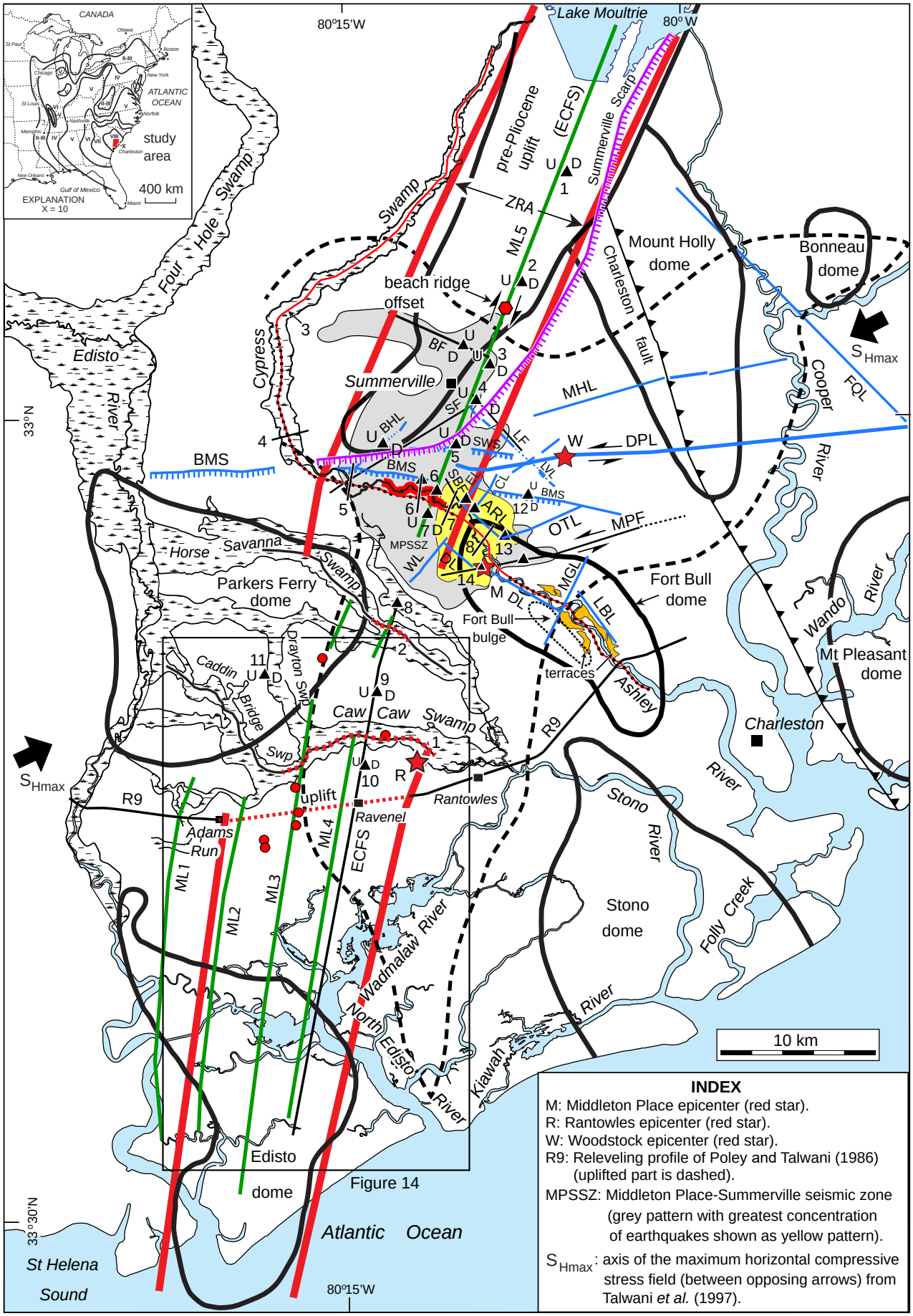

Table 1. Fault name abbreviations.

Abbreviation	Fault
ARFZ	Ashley River fault zone
BF	Berkeley fault
LF	Lincolnville fault
MPF	Middleton Place fault
SBF	Sawmill Branch fault
SF	Summerville fault

Table 2. Abbreviations for names of lineaments and scarps.

Abbreviation	Lineament or scarp
ARL	Ashley River lineament
BHL	Boone Hill lineament
CL	Coosaw Creek lineament
DL	Dawkins lineament
DPL	Deer Park lineament
EL	Eagle Creek lineament
FQL	French Quarter lineament zone
LBL	Lambs lineament
LVL	Lincolnville lineament
MS	McChune scarp
MGL	Magnolia Gardens lineament
MHL	Mount Holly lineament
OTL	Otranto lineament
SS	Summerville scarp
SWS	Summerwood scarp
WL	Waring lineament

attribute it to any known subsurface structures. Figure 2 (shaded area) shows this topographically high area interpreted from a LiDAR image of the Charleston region shown in figure 2 of Marple and Hurd (2020). Talwani (1999) modified his 1982 model in which he hypothesized that the Woodstock fault is offset 3–4 km to the southeast by the NW-SE-oriented Ashley River fault. Based on geological and geophysical data and anomalous changes in river morphology, Marple and Talwani (2000) postulated that the main shock of the Charleston earthquake occurred along the southern end of the ECFS, locally known as the Woodstock fault. Using shallow drill-hole data, Weems and Lewis (2002) hypothesized that scissors-like compression on a crustal block between a north-south-oriented Adams Run fault and the NW-SE-oriented Charleston fault causes co-seismic displacements on the Woodstock, Summerville, and Ashley River faults (Fig. 2). Marple and Miller (2006), in contrast, postulated that the 1886 Charleston earthquake was associated with a 12° restraining bend in the ECFS south of Summerville and that the MPSSZ is from displacements along the ECFS and smaller faults east of the fault bend (Fig. 1). Based on fracture data from colonial Fort Dorchester near the Ashley River, Bartholomew and Rich (2007) attributed the main shock of the Charleston earthquake to reverse displacement on a NW-SE-oriented, near-vertical Dorchester fault. Durá-Gómez and Talwani (2009) and Talwani and Durá-Gómez (2009) modified Talwani's (1999) model in which they postulated that the Woodstock fault (WF) is offset ~6 km to the southeast along the Ashley River valley and that the northern and southern segments–WF(N) and WF(S)–dip ≥ 50° to the northwest. They also postulated that the main shock of the 1886 Charleston earthquake occurred on the ~13-km-long, NW-SE-oriented, southwest-dipping Lincolnville reverse fault between WF(N) and WF(S) and that the second smaller earthquake west of Rantowles occurred on WF(S). Marple (2011) argued against an offset in the Woodstock fault based on the lack of evidence for uplift within the proposed restraining offset where a compressional pop-up between WF(N) and WF(S) would be expected. Based on seismic-reflection, seismicity, aeromagnetic, and gravity data, Chapman and Beale (2010) hypothesized that the Charleston earthquake was caused by compressional reactivation of a NE-SW-oriented early Mesozoic extensional fault. Using the results of a one-year portable seismic network that was deployed near Summerville in 2011 and 2012, Chapman *et al.* (2016) postulated that the main shock of the 1886 earthquake occurred on a ~22-km-long, N6°E-oriented reverse fault dipping ~43°W and that the MPSSZ represents aftershocks from 1886 (Fig. 2). Based on LiDAR, seismic-reflection, and surficial geologic data, Marple and Hurd (2020) postulated that the main shock in 1886 was caused by sinistral strike-slip displacement on an east-west-oriented fault associated with the ~40-km-long Deer Park lineament[1]

1 Deer Park lineament was incorrectly referred to as the Deer Creek lineament on page 86 of Marple and Hurd (2020).

Figure 2. (next page) Summary map showing seismicity recorded between 1974 and 2021 (yellow dots) (U.S. Geological Survey 2021), seismic-reflection profiles with locations of interpreted faults (black ticks, U on upthrown side), and linear magnetic anomalies ML1-ML5 (green lines). Previous interpretations of faults are grey and red lines. Light grey area in the northwest part of the area is the topographically higher area interpreted from the LiDAR data of Marple and Hurd (2020, fig. 2). The pre-Pliocene high near Summerville is shown by the thick grey contour. The incised part of the Ashley River is highlighted with thick red contour. Tables 1 and 2 show the abbreviations of faults, LiDAR lineaments (blue lines), and scarps (contours with ticks). Red dots are epicenters of small modern earthquakes east of Adams Run. Isoseismal contours of Sloan (Dutton 1889) are dashed. S1 is the location of the "ridges or permanent waves" along the Northeastern Railroad described in Dutton (1889, pp. 291). S2 is the location along the South Carolina Railroad where the direction of compressions reversed direction during the 1886 Charleston earthquake (Dutton 1889, pp. 287, 288, and 295). S3 is the location of significant S-shaped deformation of the Northeastern Railroad caused by the seismic waves during the 1886 Charleston earthquake (Dutton 1889, pp. 290).

near Woodstock (Fig. 1). They further concluded that this fault is one of several that formed to compensate for the increased compression caused by dextral displacement along a 12° restraining bend in the ECFS, referred to herein as the Summerville restraining bend (Fig. 2). Based on reprocessed seismic-reflection and aeromagnetic data and recently acquired ground penetrating radar (GPR) profiles, Pratt *et al.* (in press) interpreted several NE-SW-oriented faults deforming the Cretaceous and younger Coastal Plain strata in the epicentral area of the Charleston earthquake.

A major weakness of most of these hypotheses is that they attributed the 1886 Charleston earthquake to a single fault rupture, despite the evidence for at least two fault ruptures as previously discussed. Our goal was to reevaluate legacy aeromagnetic, LiDAR, and seismic-reflection data and surficial geologic maps to evaluate evidence for and against the existence of the ECFS and faults associated with the Summerville restraining bend.

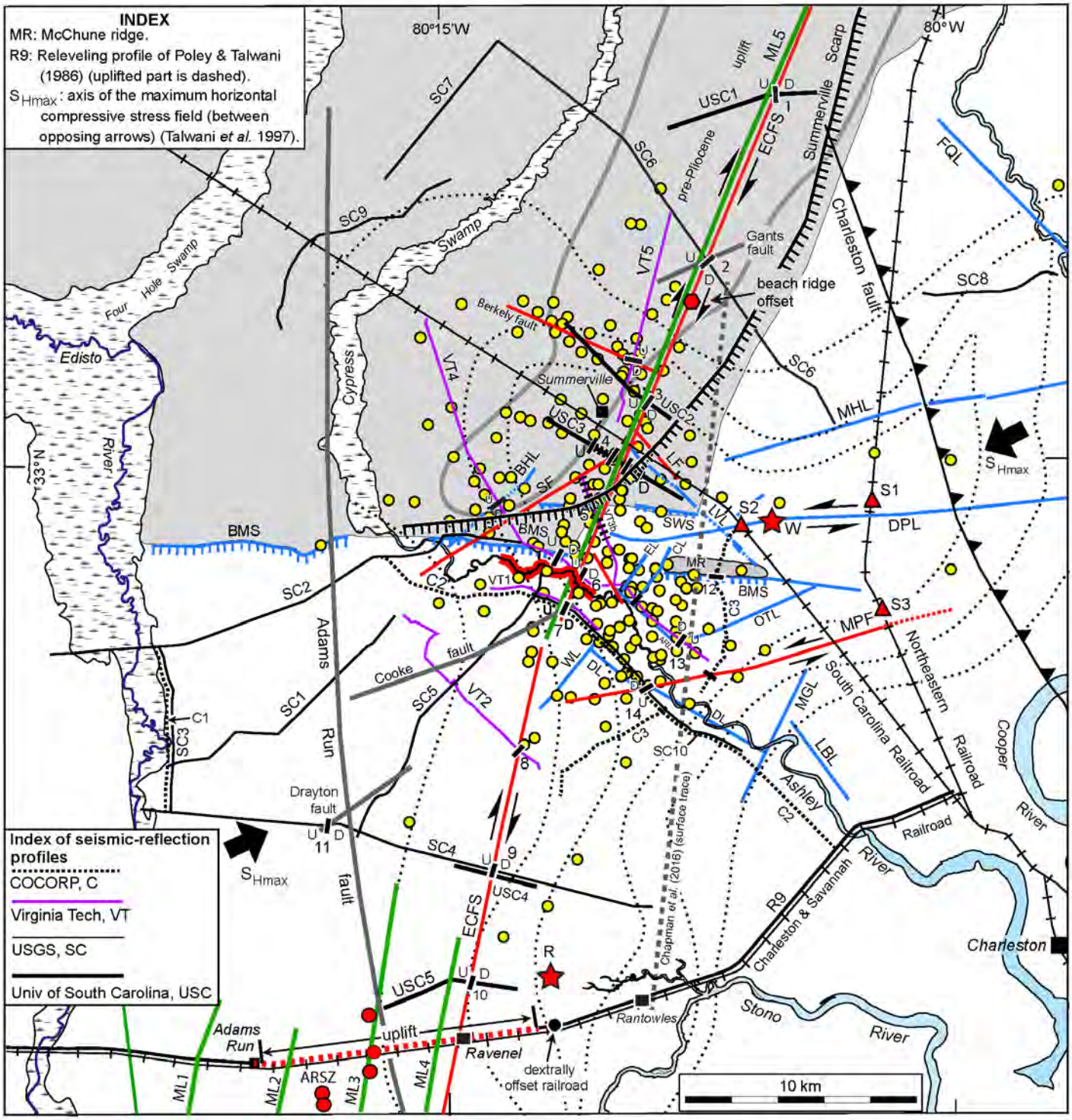

Initial aeromagnetic studies of the Charleston region

Initial aeromagnetic studies of the Charleston region (Popenoe and Zietz 1977; Phillips 1977, 1988; Daniels *et al.* 1983), combined with other geophysical and deep corehole data (Rankin 1977; Gohn 1983), revealed that the thick sedimentary wedge beneath the South Carolina Coastal Plain is underlain by the South Georgia Triassic rift basin, several early Mesozoic mafic and ultramafic plutons, and numerous N-S- and NW-SE-oriented early Mesozoic diabase dikes. Phillips (1988) used edge-enhanced grey-scale aeromagnetic images illuminated from the northwest to map buried early Mesozoic border faults and diabase intrusions. Figure 3 is a portion of his aeromagnetic image in the Charleston region that he digitally enhanced in 1988 (J.D. Phillips 2020 written communication). He interpreted a ~50-km-long, NNE-SSW-oriented aeromagnetic lineament between Summerville and the Santee River (Fig. 2, ML5) that Marple and Talwani (2000) postulated is associated with the ECFS. The aeromagnetic data of Daniels (2005) used in this study are discussed later in the Methods section.

Previously mapped faults in the Charleston region

Seismic-reflection studies of the Charleston region have revealed a number of buried faults offsetting Cretaceous and younger strata beneath the outer Coastal Plain. Using Vibroseis seismic-reflection data, Hamilton *et al.* (1983) interpreted the west-dipping Gants fault on United States Geological Survey (USGS) profile SC6 northeast of Summerville and the west-dipping Cooke and Drayton faults on profiles SC4, SC5, and SC10 southwest of Summerville (Figs. 2 and 4). Marple and Talwani (2000) later reinterpreted the Gants and Cooke faults on lines SC6 and SC10 to be associated with the ECFS. Hamilton *et al.* (1983) also interpreted a ~7-km-wide "zone of missing J" on profiles SC4 and SC10 in which the J reflection (Jurassic basalt layer) is weak or missing. Marple and Miller (2006, fig. 13) interpreted a small,~10 ms (two-way travel time, TWTT) west-side-up offset of the J horizon along the western edge of this zone at CDP 285 on seismic line USC4 and concluded that the J horizon continues ~1.5 km farther to the east than on profile SC4. Farther east, the reflector amplitudes on line USC4 are much weaker like those on profile SC4. One possible explanation for the weaker amplitudes is that a change in surficial sediments across this zone could have dampened the signal strength during data acquisition. However, surficial geologic maps of this area (e.g., Weems *et al.* 2014) do not show such a change above this zone. Alternatively, the weak reflections to the east could be from minor fracturing in this zone. Diffractions near the east end of line SC4 (Hamilton *et al.* 1983) support minor faulting within this zone. Reprocessing of seismic-reflection profile SEISDATA4, an industry line that overlaps profile SC4, also supports minor faulting of the J horizon across the zone of missing J (Buckner 2011).

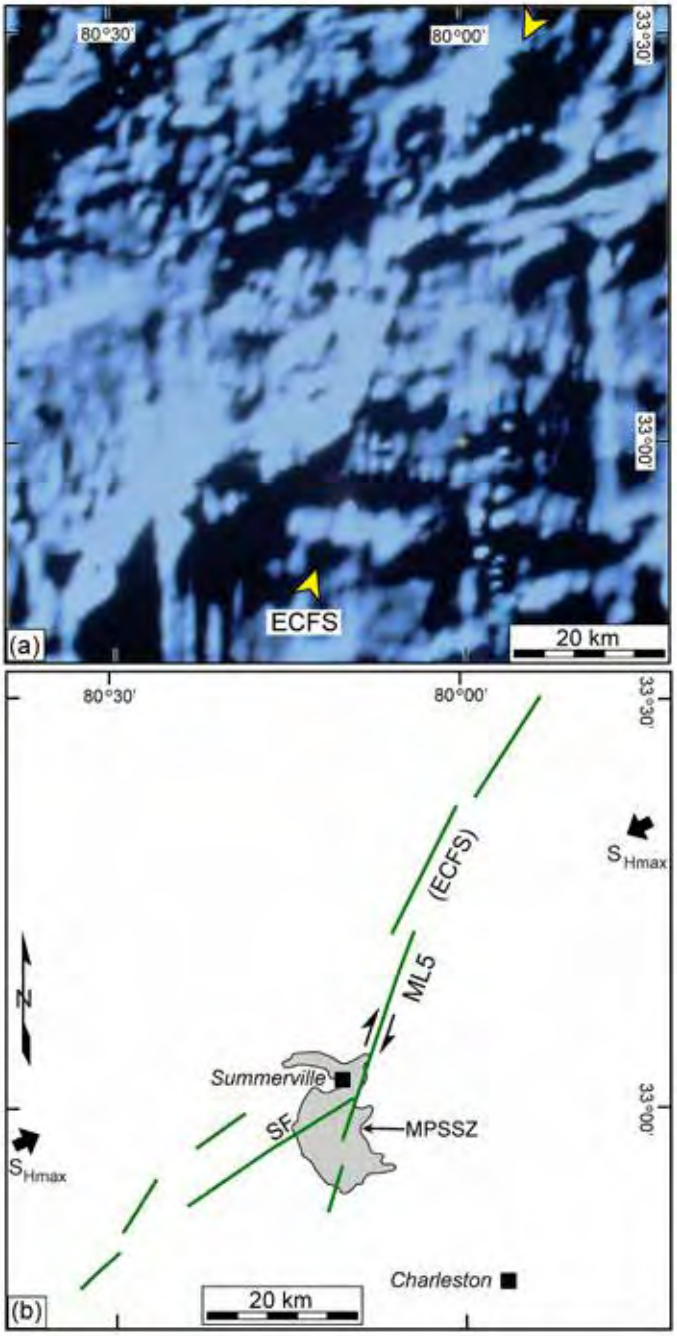

Figure 3. (a) Grey-scale aeromagnetic image of the Summerville, South Carolina, area digitally enhanced and illuminated from the northwest by J.D. Phillips (2020 written communication). Brighter areas indicate greater magnetic intensities. (b) Map for image (a). Green lines are linear aeromagnetic anomalies (e.g., ML5). SF is the Summerville fault.

The Kansas Geological Survey, in collaboration with the University of South Carolina, acquired four other seismic- reflection profiles (denoted USC) across the proposed ECFS using the Mini-Sosie and 8-gauge shotgun

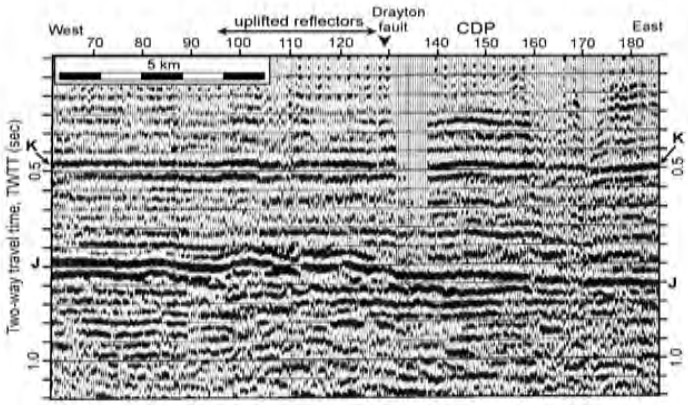

Figure 4. Part of USGS seismic-reflection profile SC4 showing the Drayton fault of Hamilton *et al.* (1983) and the uplifted J horizon. CDP is central depth point. Modified from Hamilton *et al.* (1983). Interpreted horizons: K – Upper Cretaceous, J – Jurassic basalt layer. Location of profile is shown in Figure 2.

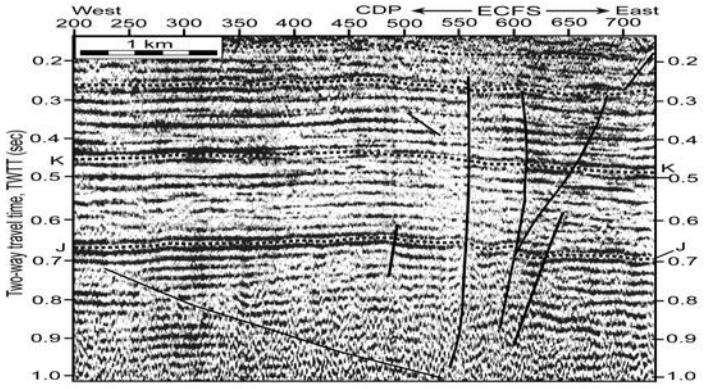

Figure 5. Interpreted seismic-reflection profile USC1 across the interpreted East Coast fault system (ECFS). CDP is the central depth point. Figure 4 caption defines J and K reflectors. Note the ~4-km-wide uplift of the horizons across the ECFS. Modified from Marple and Miller (2006). Unlabeled dashed lines are arbitrarily chosen Cenozoic horizons. Location of profile is shown in Figure 2.

methods (Marple and Miller 2006) (Figs. 1 and 2, locations 1, 3, 4, 9, and 10). Most of these profiles show buried steeply-dipping, west-side-up faults along the ECFS, commonly with folding of the overlying Cretaceous and Cenozoic strata (Figs. 5 and 6). Marple and Miller (2006) also interpreted a strike-slip fault along profile VT2 (Fig. 1, location 8, CDP 485) that was acquired by Virginia Polytechnic Institute and State University (Virginia Tech, denoted VT) where it crosses the ECFS south of the Ashley River. Although no vertical displacement was observed at this location, they interpreted a steep, west-dipping fault based on a narrow zone of low coherence that diverges upward into a positive flower structure in the overlying Cretaceous and younger strata. Two other seismic-reflection profiles in northeastern South Carolina also show buried faults where they cross the ECFS (Marple and Talwani 2000, figs. 20 and 21).

Near the northern end of COCORP (Consortium for Continental Reflection Profiling) seismic-reflection profile C3 north of the Ashley River is a buried, south-dipping, ~700-m-wide Cenozoic graben in which the horizons across the graben are offset down to the south (Schilt *et al.* 1983) (Figs. 1 and 2, location 12, and Fig. 7). This normal-style structure is anomalous in the eastern USA where reverse and transpressional strike-slip faulting have dominated the Cenozoic. The J horizon near the southwest end of profile C3 is offset up to the southwest ~100 m across a gap in this profile at the Ashley River valley (Schilt *et al.* 1983, fig. 9), which could be associated with the Ashley River fault of Talwani (1982). Vibroseis seismic-reflection profiles acquired by Virginia Tech near Summerville in the early 1980s revealed several other buried faults offsetting Cretaceous and younger strata (Costain and Glover 1983; Chapman and Beale 2008) (Fig. 2).

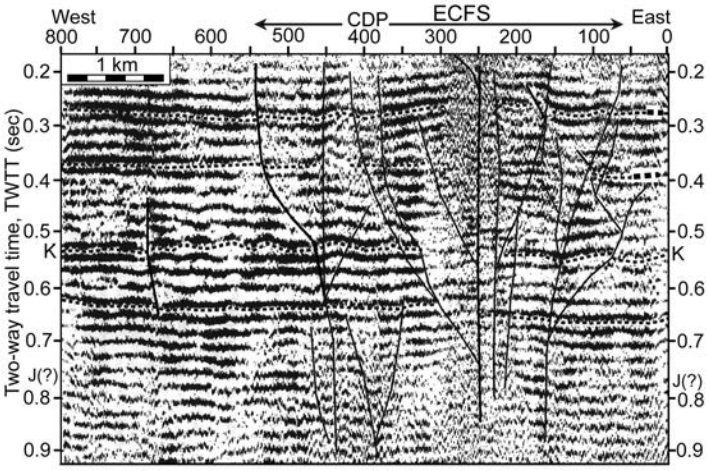

Figure 6. Interpreted seismic-reflection profile USC5 across the interpreted East Coast fault system (ECFS). CDP is the central depth point. Figure 4 caption defines J and K reflectors. Note the 3- to 4-km-wide uplift of the horizons across the ECFS. Modified from Marple and Miller (2006). Unlabeled dashed lines are arbitrarily chosen Cenozoic horizons. Location of profile is shown in Figure 2. Also note the low coherency of the reflectors approximately between CDPs 230 and 290.

Other Cenozoic faults have been mapped in the Charleston region using seismicity, aeromagnetic, shallow drill-hole, and other seismic-reflection data, including the Adams Run, Ashley River, Berkeley, Charleston, Lincolnville, Middleton Place, Sawmill Branch, and Summerville faults (Weems and Lewis 2002; Marple and Miller 2006; Talwani and Durá-Gómez 2009; Marple and Hurd 2020) (Figs. 1 and 2).

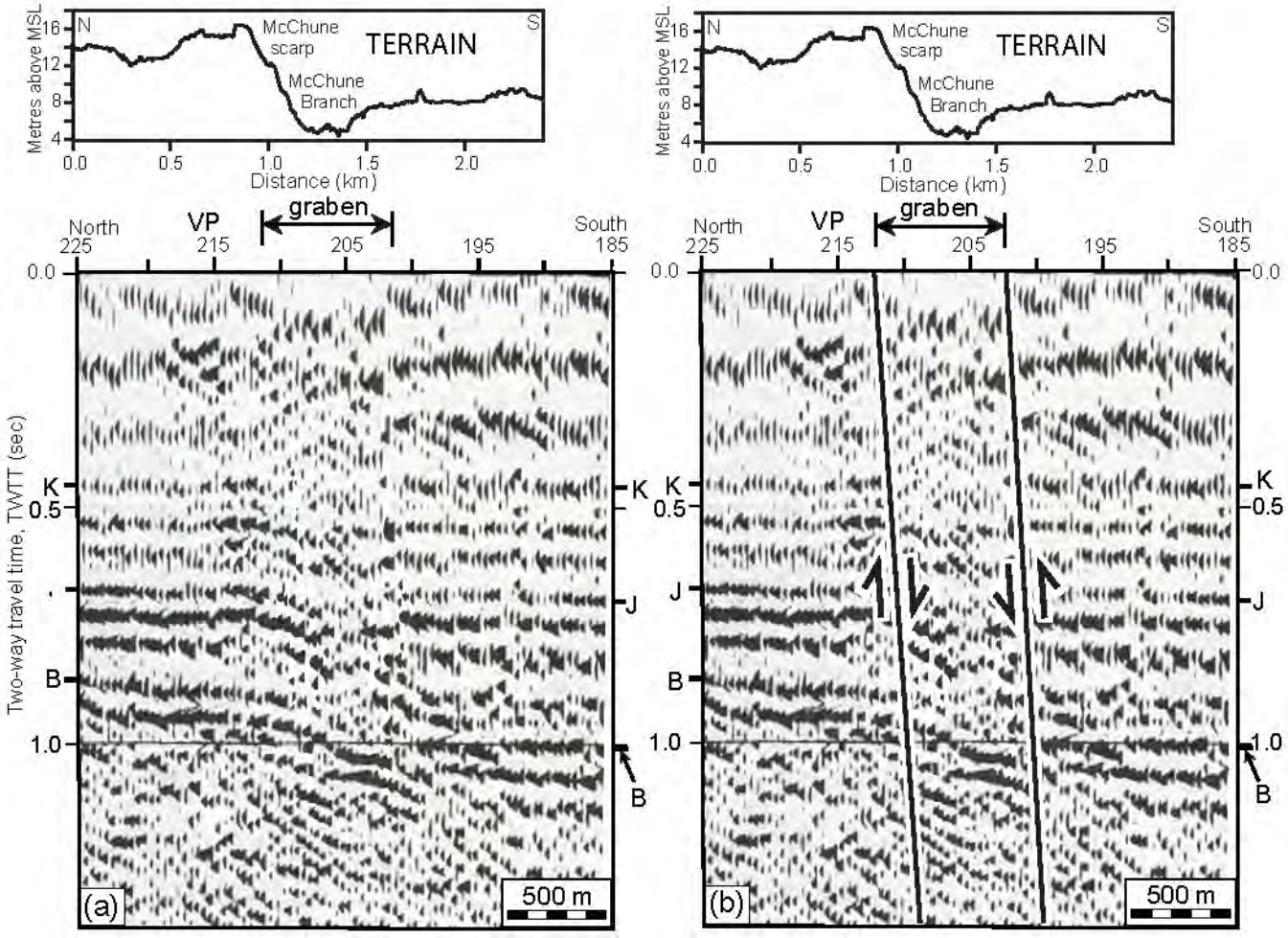

Figure 7. Part of the COCORP seismic-reflection profile C3 showing south-side-down offsets of the B (crystalline basement) and J horizons and the Cenozoic graben along the proposed McChune fault. VP is vibration point. The topographic profiles above the seismic sections are from Marple and Hurd (2020, fig. 5, profile 18). Modified from Schilt *et al.* (1983). Location of profile is shown in Figure 2.

East Coast fault system (ECFS)

Marple and Talwani (1993) interpreted a ~200-km-long buried dextral strike-slip fault system, locally known as the Woodstock fault near Summerville, in the Coastal Plain of South Carolina based on a "zone of river anomalies" (ZRA) that coincides with upwarped strata, steeply-dipping buried faults interpreted from seismic-reflection profiles, a ~50-km-long aeromagnetic lineament near Summerville (lineament ML5 in this study), and focal mechanisms of microearthquakes near Summerville that indicate dextral strike-slip motion. Marple (1994) identified a second ~200-km-long ZRA crossing the inner part of the North Carolina Coastal Plain that coincides with Cenozoic surface faults to the northeast near the Fall Line. Marple and Talwani (2000) continued this fault system into southeastern Virginia and named it the East Coast fault system (ECFS) (Fig. 1). They divided the ECFS into southern, central, and northern segments that are separated by ~10-km-wide right-step offsets. Marple and Hurd (2021) redefined the location of the central segment in southern North Carolina, thus making it continuous with the ECFS in northeastern South Carolina where it forms the 15° Cape Fear restraining bend. Uplifted Pliocene-Pleistocene fluvial terraces in the lower Cape Fear River valley in southern North Carolina (Markewich 1985; Soller 1988) and the dextral offset in the Brownsville Pleistocene beach ridge northeast of Summerville (Marple and Hurd 2020) (Fig. 8) suggest that deformation along the ECFS may have begun during the Pleistocene.

One of the most studied areas along the ECFS lies between the Ashley River and Lake Moultrie. Quaternary uplift along this part of the ECFS, combined with depositional and erosional processes associated with Pleistocene paleoshorelines, caused this area to be topographically higher than the surrounding areas (Marple and Hurd 2020) (Fig. 2). Pleistocene beach ridges that cross this area have been uplifted at least 4 m (Marple and Hurd 2020, figs. 12b and 13, profile 26) and the pre-Pliocene horizon at depth has been uplifted 10–15 m across the ZRA

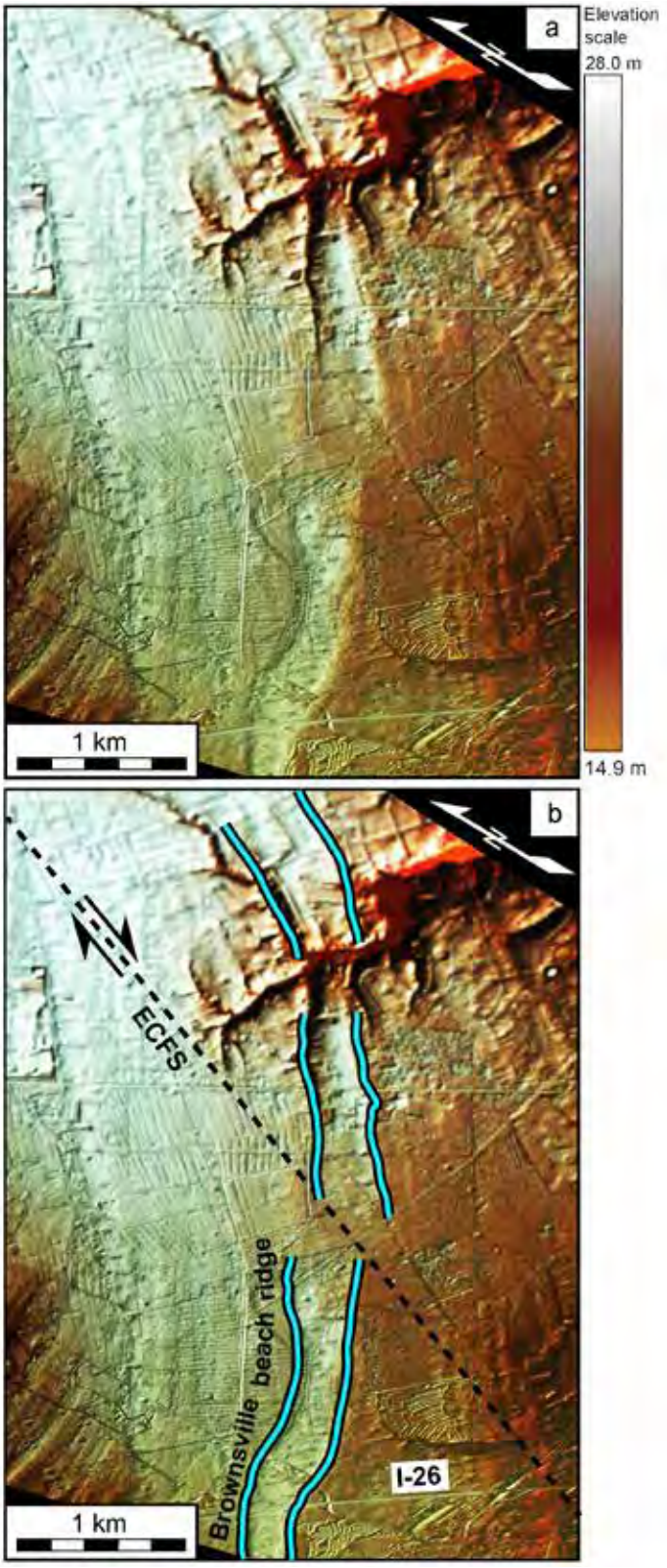

Figure 8. (a) LiDAR image of the ~320-m dextral offset in the Pleistocene Brownsville beach ridge deposit. Figure 1 shows the location of this offset. (b) Interpretation of image (a).

(McCartan *et al.* 1984, cross-section B-B'; Weems and Obermeier 1989). Changes in the age and nature of the sediments along a ~10-km-long section of the Ashley River valley floor near the southern edge of this topographic high indicate that it too has been gently uplifted during late Pleistocene or Holocene time (Marple and Talwani 1993, 2000). Here, the channel is incised 2–3 m below a late Pleistocene fluvial terrace that is underlain by sediments of the Silver Bluff and Wando formations (units *Qsbc* and *Qwc* of Weems *et al.* 2014). In contrast to this part of the river valley, the valley floor upstream is an anastomosing swamp pattern without a discrete channel and is underlain by Holocene alluvium (Cypress Swamp, unit *Qal* of Weems *et al.* 2014). Downstream from the incised part of the river the valley floor consists of Holocene tidal marsh deposits (unit *Qht* of Weems *et al.* 2014). Figure 9 is a mosaic of NAPP (National Aerial Photography Program) colour infrared photos that show this change in floodplain type along the lower Ashley River valley and Cypress Swamp. This area of interpreted uplift between Lake Moultrie and the Ashley River coincides with the ZRA (Fig. 1). Our results suggest that deformation along the ECFS and the McChune fault proposed herein may have produced this uplift.

Proposed faults associated with the Summerville 12° restraining bend

Using primarily LiDAR data, Marple and Hurd (2020) mapped a 30-km-wide area of WSW-ENE- to NW-SE-oriented lineaments and scarps east of the Summerville restraining bend (Fig. 1), which they concluded are surface expressions of faults that formed to compensate for the increased compression caused by dextral displacements along the restraining bend, including the Canter Hill, French Quarter, Mount Holly, Deer Park, Middleton Place, and Otranto lineaments. They postulated that sinistral strike-slip displacement on the ~40-km-long Deer Park lineament northeast of the bend (Fig. 1) produced the main shock of the 1886 Charleston earthquake. They based their hypothesis on the proximity of the Deer Park lineament to the Woodstock epicenter and the location along the South Carolina Railroad where compressions during the main shock reversed direction[2] (Dutton 1889, pp. 295) (Figs. 2 and 10). Marple and Hurd (2020) also noted the presence of topographic scarps that cross the ECFS just north of the restraining bend—the east-west-oriented Summerton and Bethera-McChune[3] (BMS) scarps (Fig. 2). Marple and Hurd (2020) referred to the east-west-oriented, south-facing scarp north of the incised part of the

2 The location, S2, where the direction of compressions reversed direction along the South Carolina Railroad during the main shock of 1886 was incorrectly located along the Northeastern Railroad by Weems and Lemon (1988) and Marple and Hurd (2020).

3 The Bethera-McChune scarp was previously referred to as the Summerville-McChune scarp by Marple and Hurd (2020).

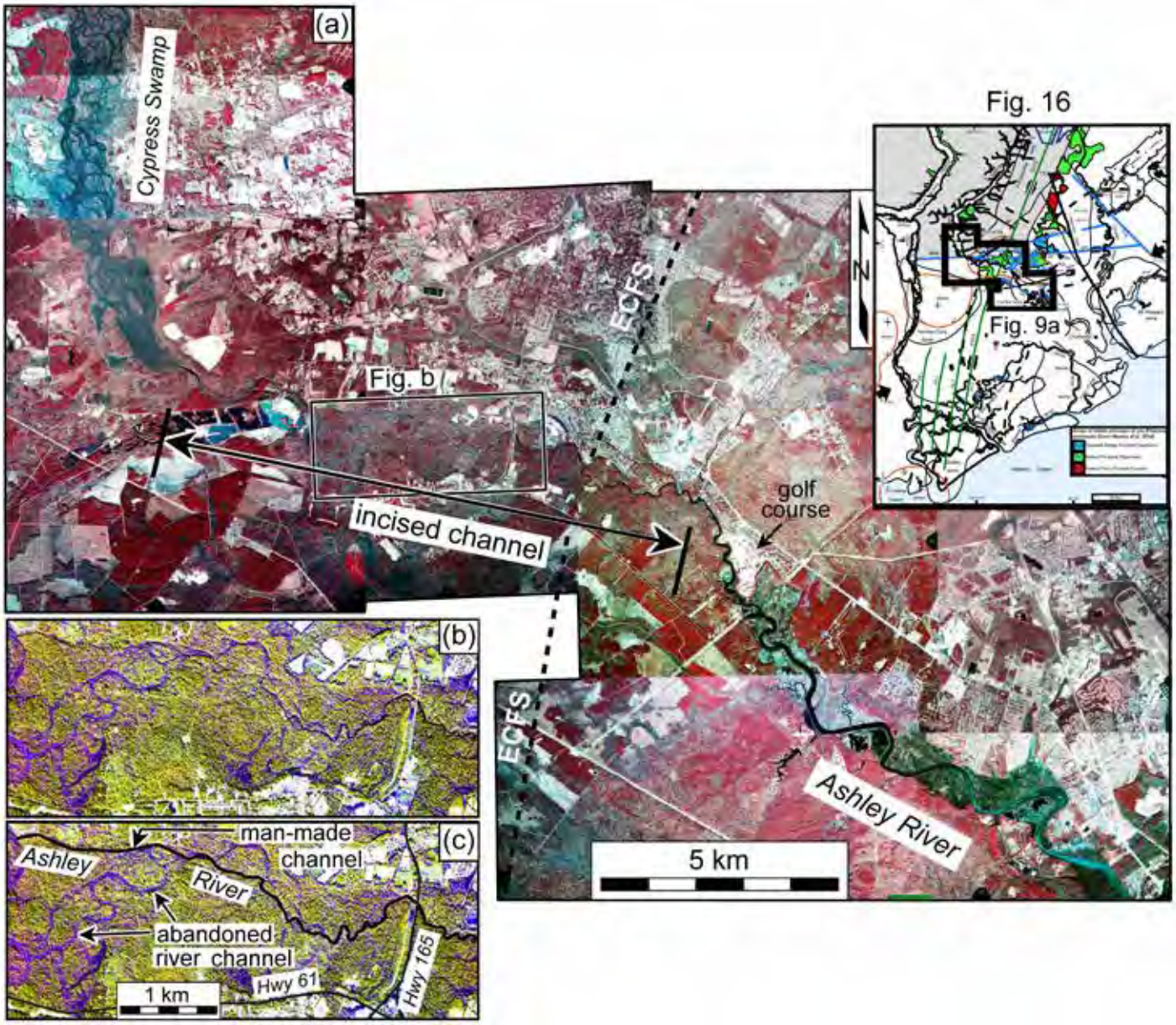

Figure 9. (a) Mosaic of NAPP colour infrared photographs acquired by the USGS in 1989 along the Ashley River valley and Cypress Swamp that shows the change in floodplain environment along the river valley where it crosses the ECFS. The Cypress Swamp upstream is dominated by an anastomosing swamp pattern whereas the floodplain to the southeast is an estuarine marsh. Between these two areas the floodplain is dominated by forested, late Pleistocene terraces. (b) IHS-enhanced subset of the mosaic along the western part of the Ashley River showing the man-made river channel and abandoned meandering channels. Location is shown in diagram (a). (c) Interpreted version of diagram (b). Location map in the upper right is from Figure 16.

Ashley River as the Summerville scarp, which is actually the Bethera scarp, whereas the Summerville scarp crosses the area 1–1.5 km to the north (Doar 2014) (Fig. 1). We, therefore, collectively refer to the two topographic scarps north of the Ashley River and McChune Branch of the Bluehouse Swamp as the Bethera-McChune scarp (BMS). Small-displacement buried faults along seismic-reflection profiles SC10 and VT3b coincide with the Middleton Place, Otranto, Eagle Creek, and Coosaw Creek lineaments (Figs. 2, 11, and 12).

GEOLOGIC AND SEISMOTECTONIC SETTING

The 1886 Charleston earthquake occurred within the swampy, heavily forested outer Coastal Plain where sea-level changes during the Pliocene and Pleistocene have produced a series of terraces underlain by emergent marine

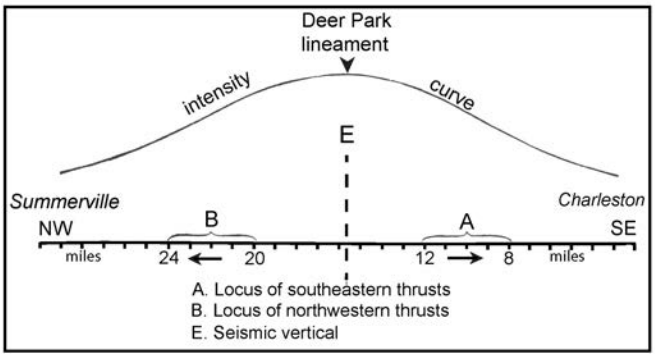

Figure 10. Location of the Deer Park lineament compared with the intensity curve of Dutton (1889) along the South Carolina Railroad that he derived for the main shock of the 1886 Charleston earthquake.

landforms, including estuarine plains, back-barrier marshes, lagoonal deposits, and sandy barrier-island ridges (Colquhoun *et al.* 1991; Weems *et al.* 2014). The terraces are bounded on the seaward (southeast) side by Pleistocene paleoshoreline scarps, including the Summerville, Macbeth, and Bethera scarps near the southern and eastern edges of the Penholoway or Wicomico terrace near Summerville (Weems *et al.* 2014; Doar 2014). Pliocene-Pleistocene uplift along the ECFS caused some of the paleoshorelines in the outer Coastal Plain to develop along and just east of the ECFS between the Ashley and Lynches rivers (Marple and Talwani 2000, fig. 12).

Nine of the near surface formations in the Charleston region are described in Table 3 because they are integrated later with some of the geomorphic observations. Exposures of the older, pre-Pleistocene sediments in fluvial valleys crossing the Charleston region could indicate Quaternary uplift. The late Eocene Parkers Ferry Formation, for example, is commonly 50–150 ft (15–50 m) beneath many areas of the Coastal Plain (e.g., Weems *et al.* 2014). Beneath the Coastal Plain sediments is a coastward-thickening, 700- to 1100-m-thick wedge of Cretaceous and Cenozoic, mostly unlithified sediments interbedded with weakly lithified to indurated sedimentary rocks that unconformably onlap and bury early Mesozoic rift basins and pre-Mesozoic terranes (Daniels *et al.* 1983; Gohn *et al.* 1983).

Modern seismicity in the Charleston region

Hypocentral depths of microearthquakes in the MPPSZ (Fig. 2) range from 1 to 12 km (Madabhushi and Talwani 1993; Chapman *et al.* 2016). Studies of focal mechanisms from the MPSSZ show a wide variety of fault types and orientations (Madabhushi and Talwani 1993; Chapman *et al.* 2016) that Marple and Hurd (2020, fig. 14) postulated is from small displacements along several faults east of the Summerville restraining bend. Chapman *et al.* (2016), in contrast, attributed the MPSSZ to aftershocks from the 1886 Charleston earthquake. However, because little modern seismicity has been recorded near the Woodstock or Rantowles epicenters, the MPSSZ may not accurately reflect the faults that ruptured in 1886.

Cenozoic structural domes in the Charleston region

Several Cenozoic structural domes have been mapped in the Charleston region using shallow drill-hole data (Fig. 1). Weems and Lewis (2002, fig. 14), for example, interpreted two such domes west of Charleston that they combined into a ~70-km-long, NNW-SSE-oriented Parkers Ferry-Edisto dome (based on structure contours of the base of the Ashley Formation) that is bounded along its eastern side by a west-dipping Adams Run fault (Figs. 1 and 2). Marple (2011) postulated that the ~20-km-long Edisto dome is a separate dome that was produced by Cenozoic uplift along the ECFS. Weems and Lewis (2002) also interpreted the Mount Holly and Mount Pleasant domes that they attributed to uplift along the upthrown (northeast) side of the Charleston fault (Colquhoun *et al.* 1983; Lennon 1985) (Fig. 1). Southeast of Summerville are the NW-SE-oriented Fort Bull bulge and dome (Weems and Lewis 2002) that are associated with uplift along the southwest-dipping, NW-SE-oriented Ashley River reverse fault (Talwani 1982; Weems and Lemon 1988) (Fig. 1). Other structural domes in the Charleston region include the Stono and Bonneau domes (Weems and Lewis 2002) (Fig. 1).

METHODS AND DATA USED

The aeromagnetic data that we used for this study were acquired from the digital aeromagnetic data of South Carolina (Daniels 2005) (Fig. 13). This map consists of eleven separate aeromagnetic surveys flown between 1958 and 1978 at 500 ft (~150 m) above ground and at a 1-mile (~1600 m) flight line separation (Daniels 2005). Flight line directions were north-south in the central part of the study area and east-west in the rest of the area. The data were reduced to the pole in order to center the anomalies over their sources (Daniels 2005). Daniels (2005) performed strike filtering in the direction of the flight lines to reduce edge effects. He then re-gridded the data to an interval of 400 m using a minimum curvature gridding algorithm and continued the data upward to 1000 feet (~305 m) above ground.

We used the Hillshade tool of ArcGIS to generate shaded relief images of Daniels' (2005) aeromagnetic data using various illumination directions, an elevation angle of 35°, and a vertical exaggeration of 30×. The data were colorized based on variations in magnetic intensities. Basic contrast enhancement routines of Adobe Photoshop were used to further enhance the aeromagnetic images, including the intensity-hue-saturation (IHS) routine. Magnetic intensity scales were not generated for the IHS-enhanced images because the IHS enhancement significantly changed their

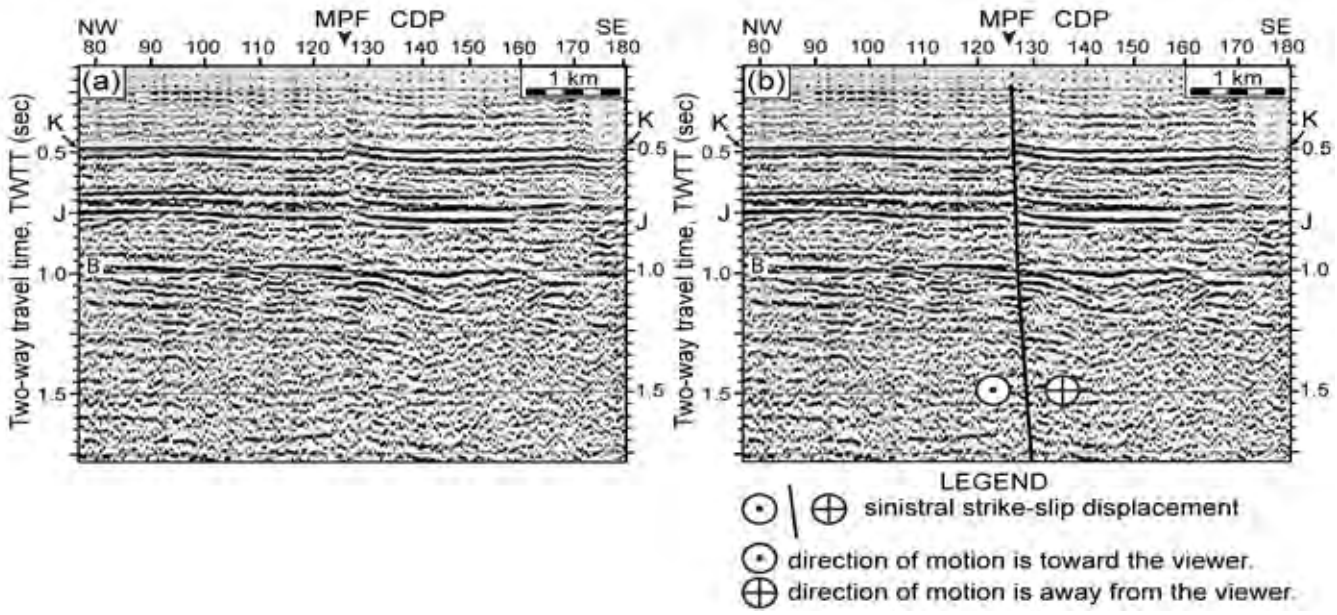

Figure 11. (a) Part of the USGS seismic-reflection profile SC10 of Hamilton *et al.* (1983) showing offsets in Cenozoic strata along the interpreted Middleton Place fault. CDP is central depth point. (b) Interpreted version of profile in diagram (a). Modified from Hamilton *et al.* (1983). Note the diffraction projecting from the fault plane just below 1.0 sec TWTT. Location of profile is shown in Figure 2.

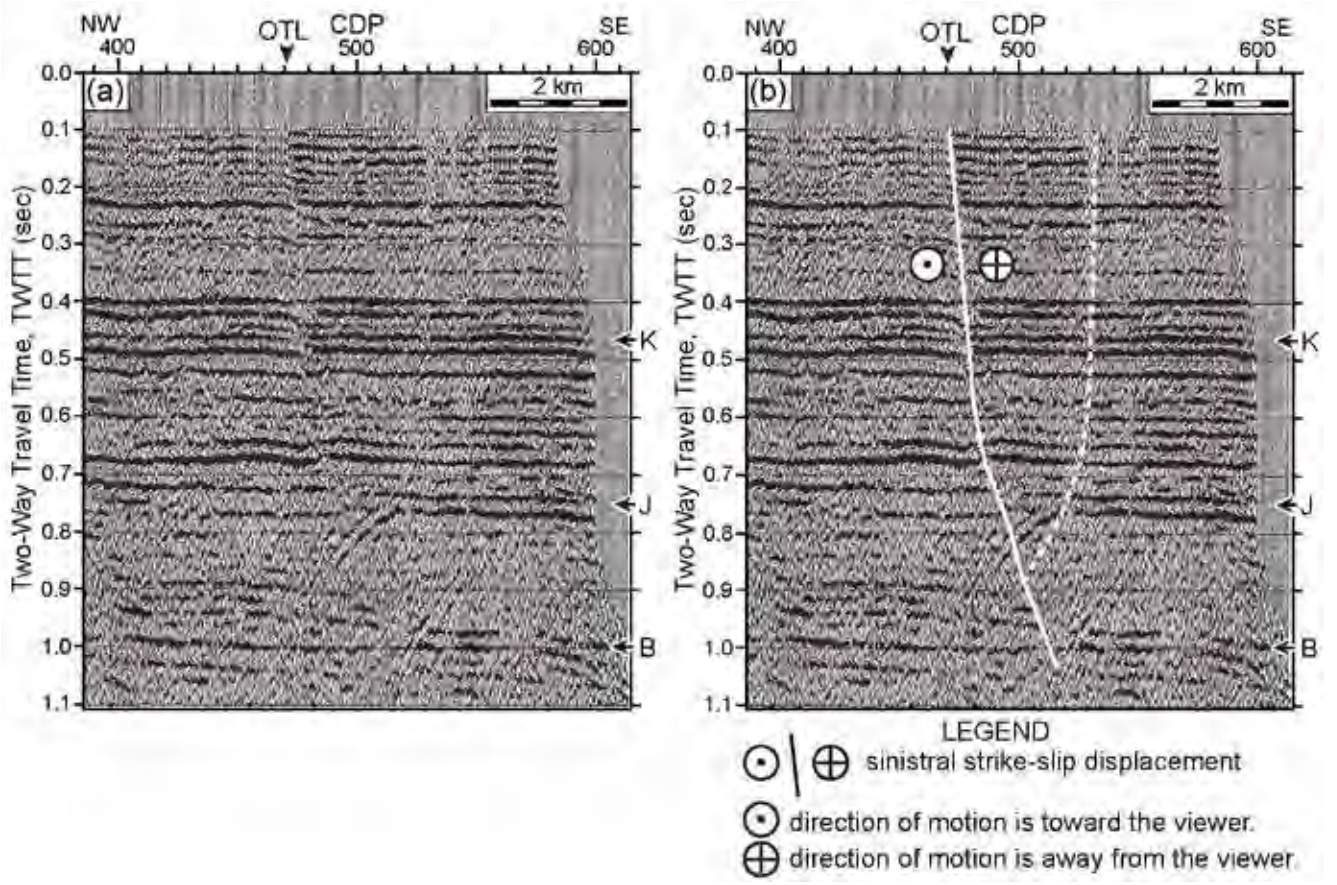

Figure 12. (a) Part of the Virginia Tech seismic-reflection profile VT3b showing offsets in the Cenozoic strata along the Otranto lineament of Marple and Hurd (2020). CDP is central depth point. (b) Interpreted version of profile in diagram (a). Modified from Chapman and Beale (2008). Location of profile is shown in Figure 2.

Table 3. Surficial deposits in the Charleston region discussed in the text.

Unit name	Unit age	Unit description and depositional environment
Parkers Ferry Formation[1,2]	Late Eocene (~36 Ma)	Stiff to plastic, dense and sticky calcilutite to fine-grained calcarenite that formed in a soft-bottomed, shallow-marine-shelf environment.
Ashley Formation[3]	Early Oligocene (~29 Ma)	Dense, erosion-resistant, weakly cemented, light-olive-brown, phosphatic and quartzose calcarenite that accumulated in an open-marine-shelf environment.
Chandler Bridge Formation[4]	Late Oligocene (~27 Ma)	Soft and easily eroded, medium-gray to dusky-green quartz phosphate sands that accumulated in a shallow-marine-shelf environment.
Raysor Formation[3]	Late Pliocene (~3.0 Ma)	Bluish-grey, shelly, clayey, and silty quartz sand that accumulated in a shallow-marine-shelf environment.
Penholoway or Wicomico Formation[2]	Early Pleistocene (Penholoway: 730–970 ka; Wicomico: 1.8–2.12 Ma)	Sand, clayey sand, and clay deposited in barrier, open lagoonal, and shallow-shelf-marine environments, especially the barrier and back-barrier complex near Summerville.
Ladson Formation[2]	Middle Pleistocene (240–730 ka)	Barrier sand and clayey sand and clay facies deposited in fluvial, estuarine, and lagoonal environments.
Ten Mile Hill beds[2]	Late Pleistocene (200–240 ka)	Poorly consolidated, easily eroded clays and clayey sands deposited in back-barrier and shallow shelf environments.
Wando Formation[2]	Late Pleistocene (70–130 ka)	Poorly consolidated, easily eroded sand, clayey sand, and clay that were deposited in fluvial, barrier, back-barrier, and estuarine marsh environments.
Silver Bluff beds[2]	Late Pleistocene (33–85 ka)	Clayey sand and clay facies that form the fluvial terrace along the incised part of the Ashley River valley.

Unit descriptions from the references: [1]Weems and Lemon (1984); [2]Weems *et al* . (2014); [3]Weems *et al* . (1997); [4]Weems and Lemon (1988).

colour schemes. Magnetic lineaments were spatially compared with previously acquired seismic-reflection profiles to determine if they spatially coincide with faults (Fig. 1).

We also examined surficial geologic maps in the Charleston region (e.g., Weems *et al.* 2014) to search for evidence of uplift along the magnetic lineaments and the LiDAR lineaments of Marple and Hurd (2020). Local exposures of older pre-Pleistocene strata, like the Parkers Ferry, Ashley, Chandler Bridge, and Raysor formations, along stream valleys could indicate areas of Quaternary uplift since they are normally buried beneath the younger Coastal Plain sediments.

Because anomalous changes in river morphology can reveal areas of Quaternary uplift (Schumm 1986), we examined topographic profiles constructed across the Ashley River valley and Cypress Swamp using LiDAR data to evaluate evidence for and against late Quaternary uplift across the ECFS in the southern meizoseismal area of the Charleston earthquake. We also sought possible evidence for late Quaternary uplift along the southern ECFS using longitudinal profiles constructed along the Horse Savanna and Caw Caw swamps and along the Ashley River valley and Cypress Swamp.

Although channel sinuosities can also be used to infer tectonic uplift (Schumm 1986), we did not construct a sinuosity profile along the Ashley River for three reasons. First, there is no consistent river channel upstream along Cypress Swamp due to its anastomosing pattern (Fig. 9). Second, the floodplain environment along the Ashley River valley changes from a dry forested terrace along the incised part of the Ashley River to a salt marsh downstream with a much larger channel affected by tides. Finally, recent field reconnaissance of the Ashley River channel near the western side of the incised part of the river revealed that the channel was straightened and deepened presumably during Colonial times to drain this part of the floodplain for rice farming. Old rice levees < 1 m high crossing this part of the floodplain are still preserved in this area and spoil from excavating the new channel is piled up along the edges of the artificial channel. The old meandering channels are easily observed south of the artificially straightened channel in Figure 9c.

OBSERVATIONS

Linear aeromagnetic anomalies southwest of the Ashley River

Illumination of Daniels' (2005) aeromagnetic data from various directions revealed a ~10-km-wide zone of several subtle 600- to 700-m-wide, 22- to 32-km-long, linear aeromagnetic anomalies trending ~N10°E west of Charleston that are formed mainly by a slight decrease in magnetization

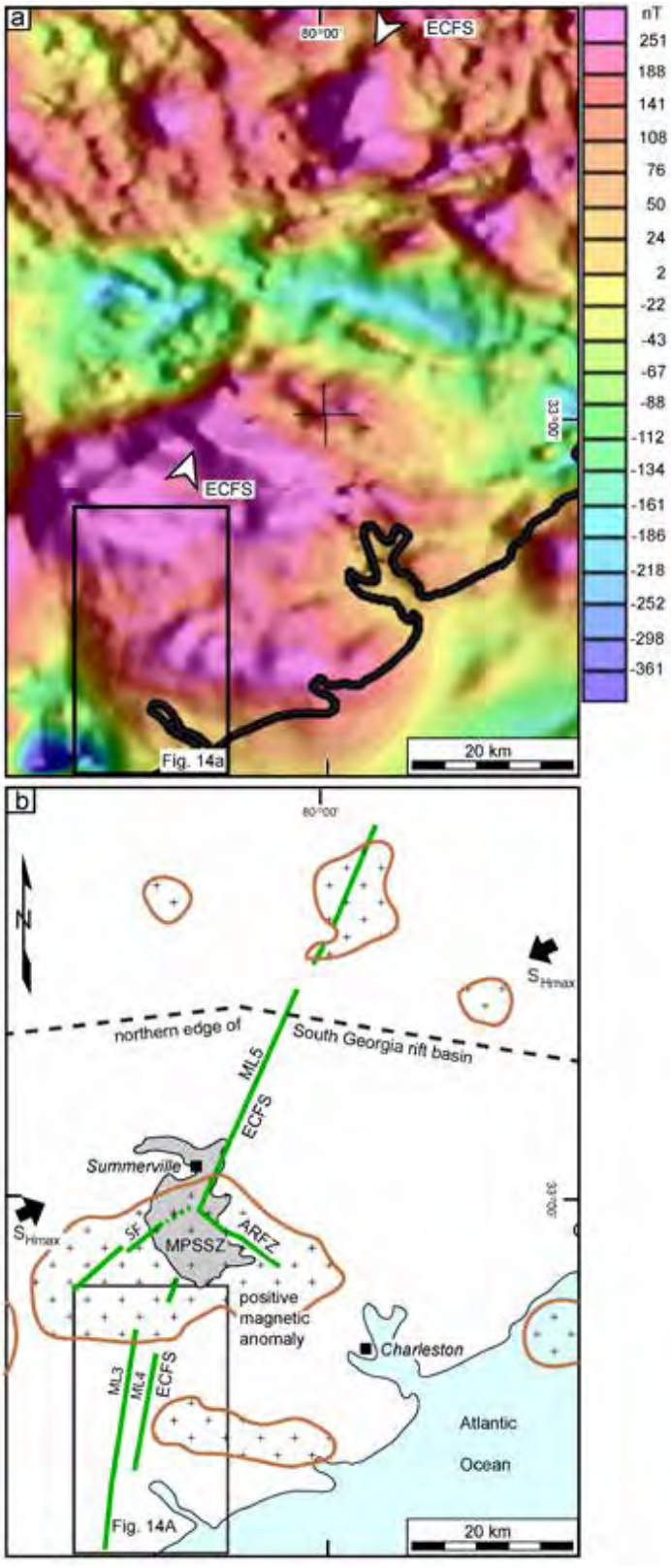

Figure 13. (a) Colour aeromagnetic image of the Charleston, South Carolina, region modified from Daniels (2005). Illumination direction is from the east. (b) Map of image (a) overlain with mafic plutons (patterned areas) in the pre-Cretaceous basement interpreted from the positive aeromagnetic anomalies in image (a).

(Figs. 1, 13, and 14, ML1-ML4). The two most prominent lineaments, ML3 and ML4, were enhanced further using the IHS enhancement and by illuminating the data from 110° (Figs. 14b–14d). The easternmost lineament, ML4, is located 1–1.5 km west of and parallels the trend formed by the buried faults along seismic-reflection profiles VT2, USC4, and USC5 (Fig. 1, locations 8–10) that define the location of the ECFS. Approximately 3 km west of ML4 is magnetic lineament ML3 that crosses the area of instrumentally-recorded earthquakes east of Adams Run (Fig. 1). Lineaments ML3 and ML4 coincide with the Edisto dome to the south and the interpreted uplifts along Caw Caw Swamp and releveling line 9 (denoted R9 in Figs. 1 and 15).

Magnetic lineaments ML1 and ML2 (Fig. 1) were optimally enhanced using the IHS enhancement and a 180° illumination azimuth. Unlike magnetic lineaments ML2-ML4, ML1 is curved (Figs. 14c and 14e). The northward projection of ML2 coincides approximately with the west-side-up Drayton fault along USGS seismic-reflection profile SC4 (Fig. 1, location 11, and Fig. 4, CDP 127). The upwarped reflectors west of this fault between CDPs 97 and 126 and at ~1 sec TWTT also coincide with the Parkers Ferry dome (Fig. 1). The northward projections of ML1 and ML3 also coincide with the east side of Parkers Ferry dome (Fig. 1).

Linear aeromagnetic anomaly ML5 along the ECFS near Summerville

Aeromagnetic lineament ML5 trends ~N22°E near Summerville (Figs. 1, 2, 3, and 13) and is located near the trend formed by several buried, steeply-dipping, west-side-up faults (Fig. 1, locations 1–7) and the ~320 m dextral offset in the Pleistocene Brownsville beach ridge deposit (Fig. 8). ML5 coincides with the ZRA (between thick red lines in Fig. 1) and crosses the MPSSZ, the incised part of the Ashley River (Fig. 9), and an area where the early Oligocene Ashley Formation is exposed beneath the middle Pleistocene Ten Mile Hill beds (next section) (Figs. 1,

Figure 14. (next page) (a) Enlarged image of magnetic lineaments (arrows) west of Charleston taken from Daniels (2005), which he illuminated from the east. Figure 13a shows the location of image (a). (b) IHS-enhanced version of image (a) illuminated from 110°. (c) IHS-enhanced version of image (a) illuminated from 180°. (d) Image (b) enhanced further with additional IHS enhancements. (e) Summary of lineaments interpreted from images (a)–(d).

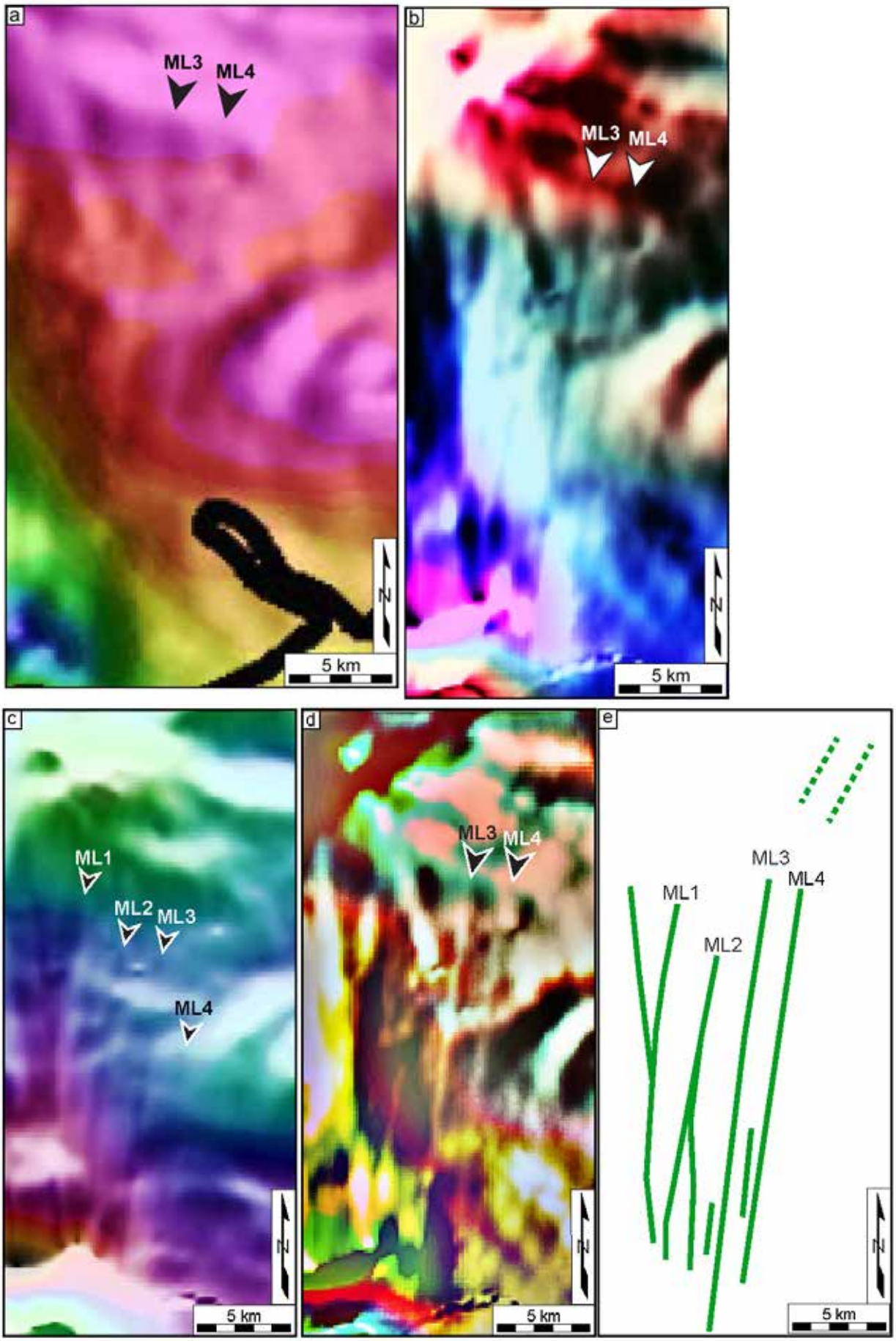

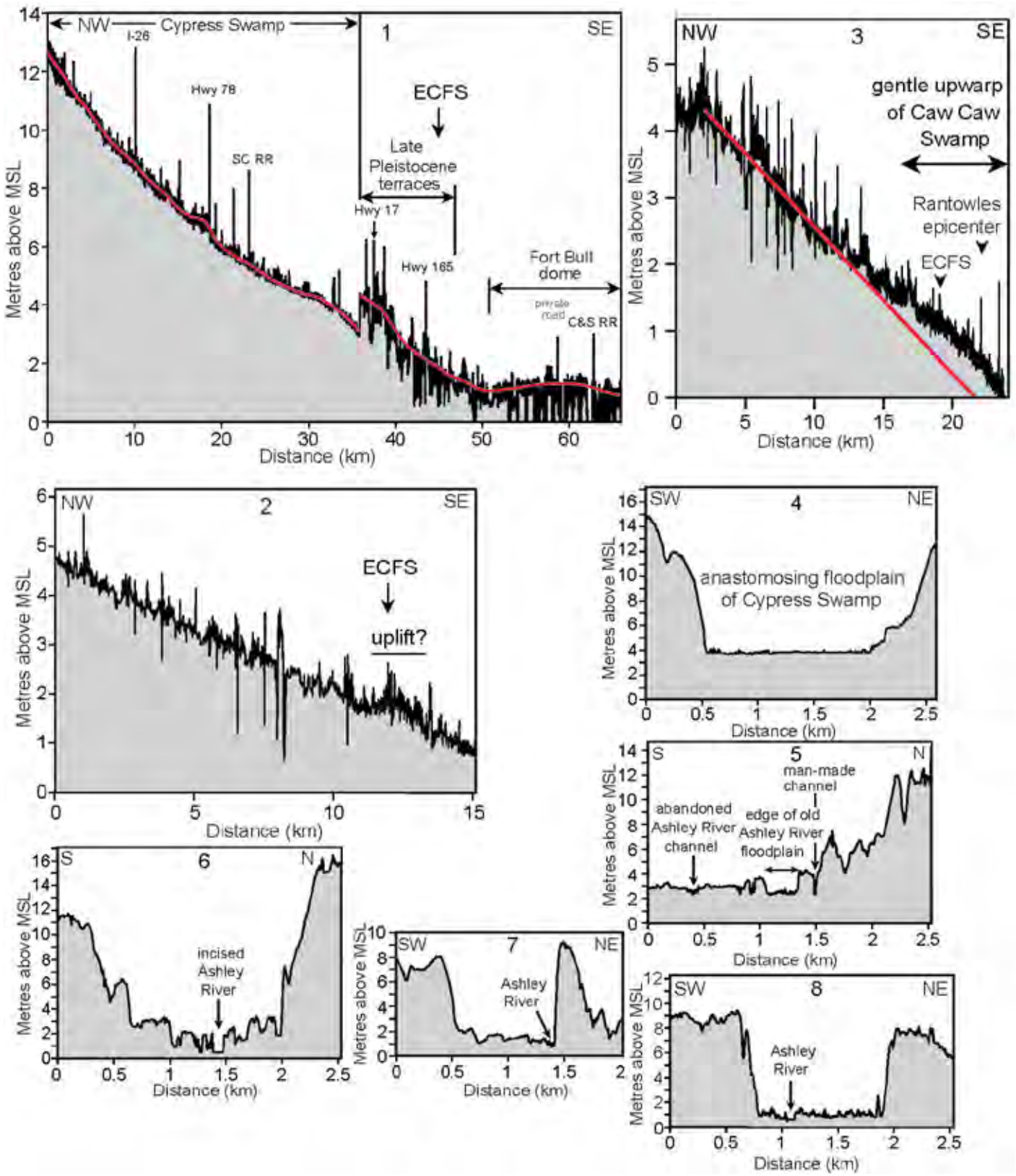

Figure 15. LiDAR-derived longitudinal profiles 1–3 along the Caw Caw and Horse Savanna swamps and the Ashley River. Red line is an arbitrary reference datum. Profiles 4–8 are LiDAR-derived profiles across the Ashley River valley and Cypress Swamp. Locations of profiles are shown in Figure 1.

16, and 17a). The trends of ML4 and ML5 intersect south of the Ashley River where they form the 12° Summerville restraining bend along the interpreted ECFS (Fig. 1).

The longitudinal profile constructed along the Ashley River valley and Cypress Swamp reveals a ~15-km-wide area that is gently upwarped upstream from the late Pleistocene terraces associated with the incised part of the Ashley River (Fig. 15, profile 1). Cross-valley elevation profiles revealed that magnetic lineament ML5 crosses the area of greatest incision, which is up to 2 m deeper than upstream or downstream (Fig. 15, profile 6). The cross-valley profile upstream across Cypress Swamp (Fig. 15, profile 4) shows that the valley floor lacks a channel, which is consistent with its anastomosing swamp pattern. Downstream, the longitudinal profile is slightly upwarped ~1 m where it crosses the Fort Bull dome (Fig. 15, profile 1).

New geomorphic and stratigraphic anomalies interpreted along the ZRA and ECFS

Investigation of LiDAR data and recently published geologic maps of the Charleston region (e.g., Weems *et al.* 2014) revealed new geomorphic and stratigraphic anomalies along the ZRA that support the existence of the ECFS. Near the coast the ZRA and ECFS coincide with the Edisto dome of Weems and Lewis (2002) (Fig. 1). North of this dome and near the Rantowles epicenter of the Charleston earthquake, the longitudinal profile along Caw Caw Swamp is gently upwarped where it crosses the ECFS and ZRA (Fig. 15b, profile 3). The valley along this part of Caw Caw Swamp is also the most deeply entrenched, up to 12 m (Marple 1994, fig. 3.4). About 6 km north of Caw Caw Swamp and near the interpreted fault along seismic-reflection profile VT2 is a ~2-km-long gently upwarped part of a longitudinal profile along Horse Savanna Swamp (Fig. 15, profile 2). Just south of the incised part of the Ashley River, the early Oligocene Ashley Formation is locally exposed beneath the middle Pleistocene Ten Mile Hill beds, yet is absent to the east and west (Weems *et al.* 2014) (Figs. 16 and 17a). The Ashley Formation is also exposed in the bed of the incised Ashley River. West of this area the LiDAR image in figure 2 of Marple and Hurd (2020) reveals that the Horse Savanna and Caddin Bridge swamps are continuous with the north-south-oriented part of the Edisto River valley to the west (Fig. 1).

New geomorphic and stratigraphic anomalies along the Bethera-McChune scarp (BMS)

The top of the early Oligocene Ashley Formation is ~14 feet (4.3 m) higher along the south-facing BMS north of the incised segment of the Ashley River than that to the south (Fig. 17a) (Weems *et al.* 2014, cross-section A-A'). Eastward, the Ashley and late Oligocene Chandler Bridge formations are exposed along the BMS along the south side of McChune ridge, yet are absent to the south (Fig. 17a). This change in elevation of the Ashley Formation also coincides with the 15- to 20-m drop in elevation south of the BMS. Beneath the McChune Branch of Bluehouse Swamp and the BMS is the ~700-m-wide, south-side-down, south-dipping Cenozoic graben on seismic-reflection profile C3 (Schilt *et al.* 1983) (Fig. 2, location 12, and Fig. 7). Between McChune Branch and Goose Creek valley to the east is a small tributary of Goose Creek that is collinear with McChune Branch. The Chandler Bridge Formation is locally exposed along this tributary (Fig. 17a). Seismic-reflection profiles VT3b and VT4 also cross the scarp trend along the 3- to 4-km-wide gap along the BMS (Fig. 1). However, profile VT3b bends ~90° to the east near the scarp and profile VT4 crosses the scarp trend at a low angle (Fig. 2) and are therefore not ideal for interpreting faults along this trend. Some fault plane solutions of microearthquakes near the BMS trend east-west where it crosses the MPSSZ (Marple and Hurd 2020, fig. 1).

Crossing the ZRA just north of the Ashley River is a discontinuous, ~20-km-long, low-lying east-west-oriented ridge, referred to herein as the Summerwood ridge, and the south-facing Summerwood scarp that cross various geologic units (Fig. 17a). They are also nearly collinear with the Deer Park lineament to the east (Fig. 17a). The western end of Summerwood ridge is capped by late Pleistocene (70–130 ka) Ladson barrier sediments (Weems *et al.* 2014) (Fig. 17a). Several horizons near the northwestern end of seismic-reflection profile VT3b are gently upwarped beneath Summerwood ridge (Chapman and Beale 2008, figs. 4 and 5, CDPs 30-150) (Fig. 2, dashed part of profile VT3b).

Anomalous outcrops of the Parkers Ferry, Ashley, Chandler Bridge, and Raysor formations in the northern Charleston region

Several of the older pre-Pleistocene formations that are normally buried beneath the younger Coastal Plain sediments are anomalously exposed in numerous fluvial valleys in the northern part of the Charleston region where the terrain is higher (Fig. 16). Between the ECFS to the west, the Canterhill lineament (surface expression of the Charleston fault) to the east, and the BMS to the south (Figs. 16 and 17b) is a NNE-oriented area where the late Eocene to Oligocene Parkers Ferry, Ashley, and Chandler Bridge formations are exposed along numerous stream valleys. This area is also 5–10 m higher than the areas to the east and south (Marple and Hurd 2020, fig. 5, profiles 1 and 2) and parallels the ECFS to the west (Fig. 16). The oldest geologic unit exposed in the Charleston region, the late Eocene Parkers Ferry Formation, outcrops along several stream valleys (Weems *et al.* 2014) where they cross the northwestern end of the Mount Holly dome and the Canterhill lineament along the Charleston fault (Figs. 16 and 17b). Near Woodstock, the Ashley Formation is locally exposed along the anomalous horse-shoe-shaped Blue-

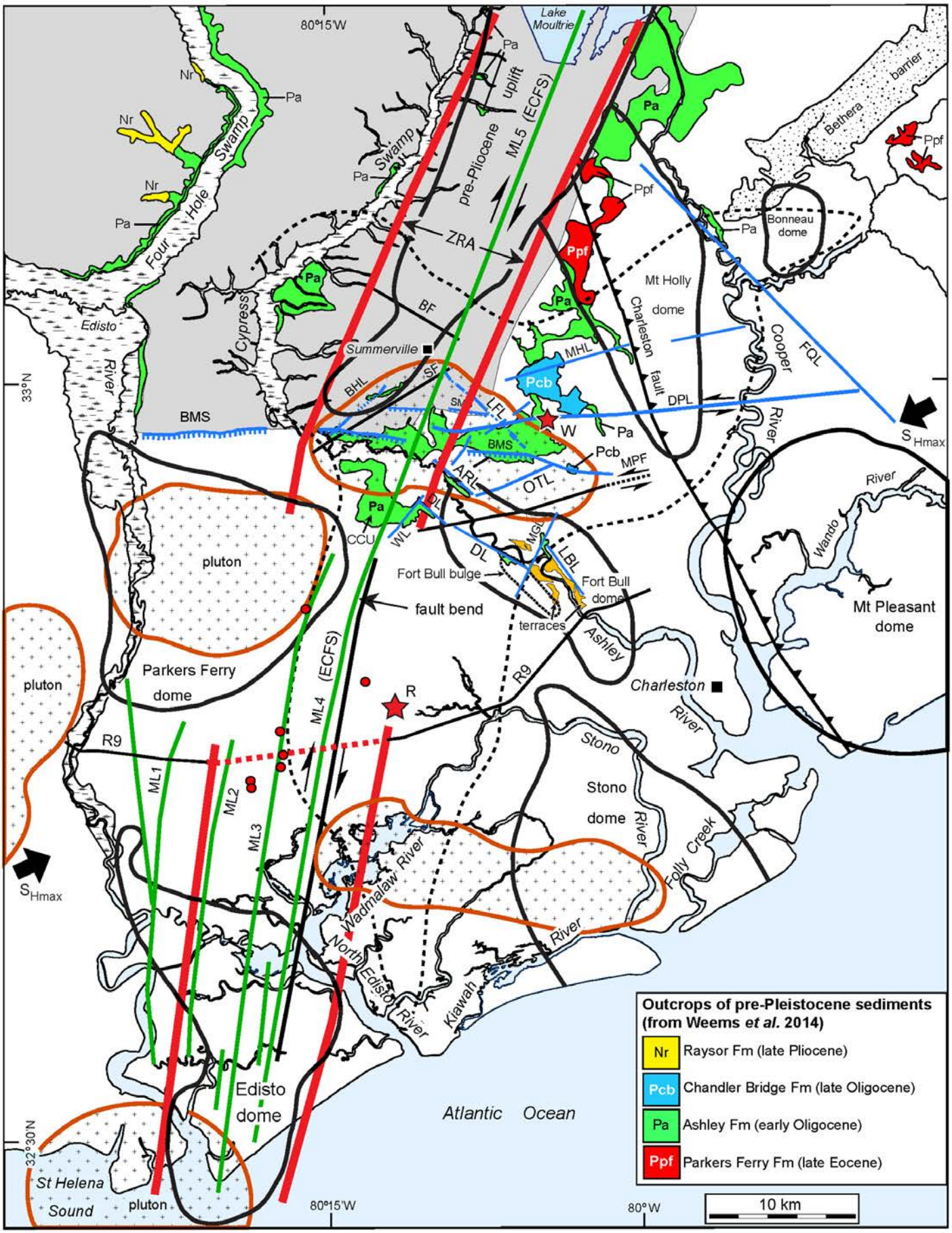

house and Goose Creek swamps where they intersect the Deer Park lineament (Fig. 17a).

Along some of the tributaries of the East Branch of the Cooper River and ~7 km northeast of Bonneau dome are other anomalous exposures of the late Eocene Parkers Ferry Formation (Fig. 16). The early Oligocene Ashley Formation is also locally exposed along an ~5 km long reach of the North Branch of the Cooper River valley where it coincides with the NW-SE-oriented French Quarter lineament (Fig. 17b). North of the BMS and west of the ZRA are exposures of the Ashley and late Pliocene Raysor formations along the Edisto River valley and the Four Hole and Cypress swamps (Figs. 16 and 17b).

Outcrops of the Ashley Formation along the Ashley River valley south of the BMS

The early Oligocene Ashley Formation outcrops along various segments of the Ashley River valley south of the BMS where they coincide with the NW-SE-oriented Ashley River, Dawkins, and Lambs lineaments of Marple and Hurd (2020, fig. 14). For example, northwest of Middleton Place and along the Ashley River lineament (ARL) of Marple and Hurd (2020) are exposures of the Ashley Formation that are absent on the opposite side of the valley (Figs. 16 and 17a). The ARL also crosses the greatest concentration of micro-seismicity in the MPSSZ (Marple and Hurd 2020, fig. 14) (Figs. 1 and 2).

The Ashley Formation also outcrops southeast of Middleton Place along the southwest side of the Ashley River valley for ~2 km (Weems *et al.* 2014) (Fig. 16). These outcrops coincide with the Dawkins lineament[4] where it crosses the Fort Bull dome (Fig. 16). The J horizon on seismic-reflection profile C3 beneath this part of the river valley is ~100 m higher to the southwest (Schilt *et al.* 1983, fig. 9).

Southeast of the NNE-SSW-oriented Magnolia Gardens lineament are exposures of the Ashley Formation along both sides of the Ashley River valley that coincide with the Pleistocene terraces of Marple and Hurd (2020, fig. 3) (Figs. 1 and 16). The outctrops along the northeast side of this part of the valley coincide with the Lambs lineament of Marple and Hurd (2020). This part of the Ashley River valley also coincides with the Fort Bull dome and is just northeast of the Fort Bull bulge (Fig. 16).

4 The Dawkins lineament was incorrectly referred to as the Dawson lineament by Marple and Hurd (2020).

DISCUSSION

Origin of the linear aeromagnetic anomalies

Although aeromagnetic lineaments ML3 and ML4 are conspicuously linear (Fig. 14b), it is unlikely that they are edge effects between flight paths because they trend N10°E whereas edge effects from the north-south flight paths would trend N0°E. Edge effects would also produce sharp linear boundaries between flight paths whereas the lineaments are 300–600 m wide (Fig. 14b). Furthermore, lineaments ML1 and ML2 are curved (Figs. 14c and 14e). It is also unlikely that the magnetic lineaments are associated with early Mesozoic dikes in the pre-Cretaceous basement because the nearest early Mesozoic dikes to the northwest are associated with NW-SE-oriented positive magnetic anomalies (Daniels 2005).

Despite the subtle nature of the magnetic lineaments, other observations suggest that they are associated with low-displacement brittle faults in the pre-Cretaceous crystalline basement. First, previous aeromagnetic studies of brittle faults elsewhere (e.g., Sims 2009; Yang *et al.* 2016) suggest that the subtle decrease in magnetization along these lineaments could be from brittle faulting in the crystalline basement beneath the 700- to 1100-m-thick sedimentary wedge in the Charleston region. Yang *et al.* (2016), for example, concluded that brittle deformation and fluid infiltration along the Yingxiu-Beichuan fault in China caused hydrothermal alteration of magnetite along the fault zone, thus decreasing the magnetization along the fault trend. Second, the proximity of ML4 to the buried faults along seismic-reflection profiles USC4 and USC5 (Fig. 1, locations 9 and 10), the parallelism of the zone of magnetic lineaments with the ZRA (Fig. 1), and the coincidence of ML3 and ML4 with the Edisto dome (Fig. 1) suggest that late Cenozoic compressional deformation and displacements along the interpreted basement faults associated with lineaments ML4 and possibly ML3 locally uplifted the overlying Coastal Plain sediments, thus producing the Edisto dome and the gentle uplifts along releveling line 9 (Fig. 1) and the Caw Caw and Horse Savanna swamps (Fig. 15, profiles 2 and 3). The parallelism between ML4 and the southern part of Sloan's isoseismals of the Charleston earthquake (Fig. 1) suggests that it may represent the fault along which the second large earthquake occurred west of Rantowles in 1886. The alignment of Drayton fault on seis-

Figure 16. (previous page) Summary map showing area of oldest outcrops of pre-Pleistocene sediments and the ECFS, LiDAR lineaments of Marple and Hurd (2020, blue lines), Cenozoic structural domes of Weems and Lewis (2002, bold contours), plutons interpreted from Figure 13 (thick orange contours surrounding patterns composed of +s), magnetic lineaments interpreted from Figure 14, and the outer contour of Sloan's isoseismals of the 1886 Charleston earthquake (Dutton 1889). Thick red parallel lines represent the area of uplift interpreted along the ZRA and ECFS. Light grey area in the northwest part of the area is the topographically higher area interpreted from the LiDAR image in figure 2 of Marple and Hurd (2020). The small red dots are small earthquakes of the Adams Run seismic zone. The orange patterns along the lower Ashley River valley are Pleistocene fluvial terraces from Marple and Hurd (2020, fig. 3b). CCU is the Clubhouse Crossroads uplift interpreted herein.

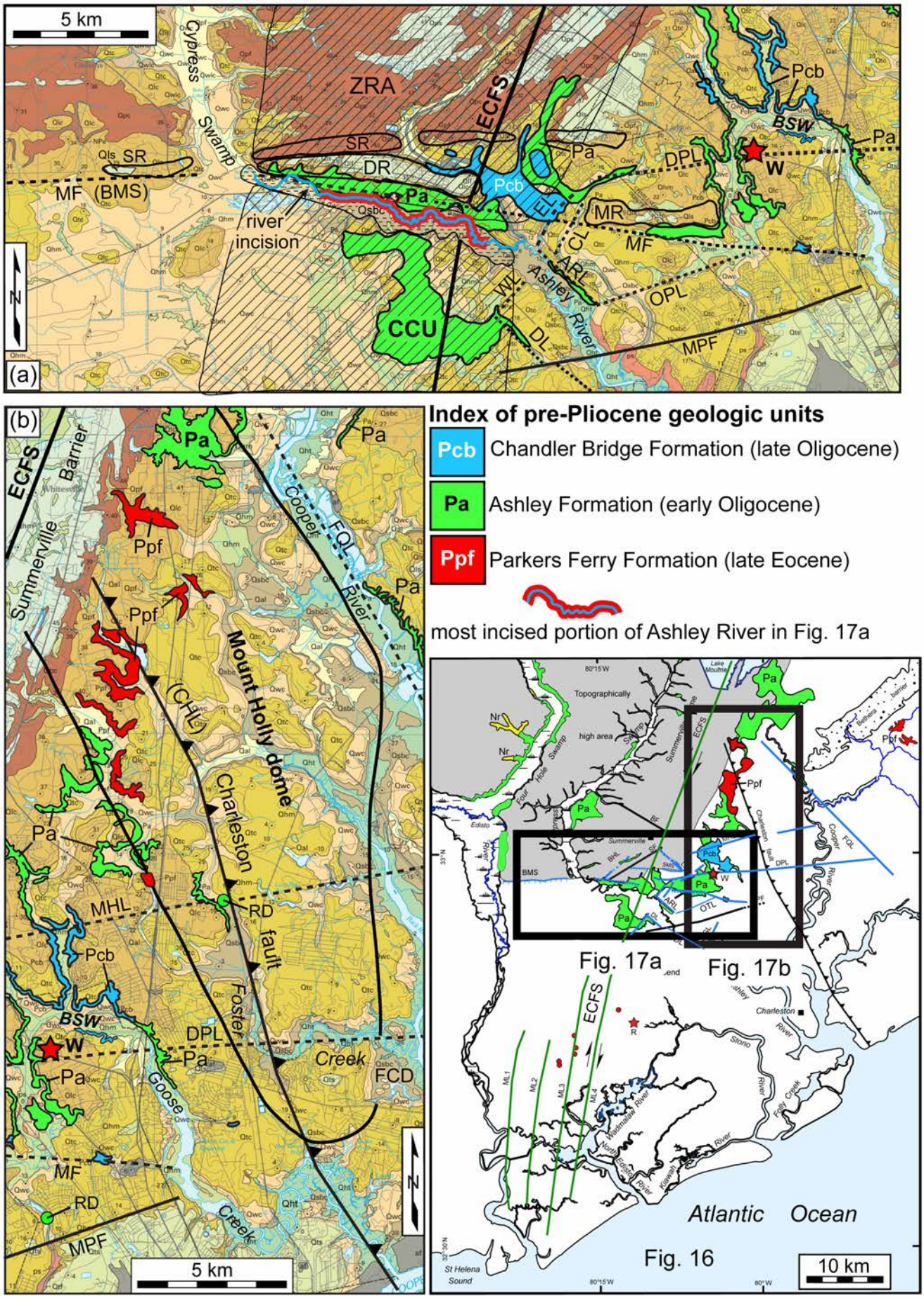

mic-reflection profile SC4 (Figs. 1 and 4) with the north-northeast projection of lineament ML2 (Fig. 1, location 11) suggests that ML2 may also be associated with a NNE-SSW-oriented fault in the pre-Cretaceous basement, uplift along which may have produced the Parkers Ferry dome (Fig. 1). The proximity of ML3 to the instrumentally recorded microearthquakes east of Adams Run (Fig. 1) suggests that it too may be a Cenozoic brittle fault in the pre-Cretaceous basement.

The continuity of magnetic lineaments ML4 and ML5 and their proximity to several buried faults interpreted from seismic-reflection profiles and the dextral offset in the Brownsville beach ridge deposit (Figs. 1 and 8) suggests that they represent the principal displacement zone along the ECFS. Because of the parallelism between lineaments ML1–ML4, we postulate that the southern end of the ECFS (Fig. 1) is associated with a broad fault zone at least 10 km wide. Thus, it is possible that the second earthquake on 31 August 1886 west of Rantowles could have been produced by dextral strike-slip displacement along the ECFS or a secondary fault east of and parallel to the ECFS.

Origin of the stratigraphic and geomorphic anomalies along the ECFS and ZRA

The anomalously thick exposures of Ashley Formation sediments along the BMS just north of the incised part of the Ashley River (Weems *et al.* 2014) (Fig. 17a) suggest that the outcrops north of the Ashley River have been exposed by late Quaternary uplift along the ECFS. The exposures of the Ashley Formation along and south of the incised part of the Ashley River valley and their absence to the east and west (Figs. 16 and 17a) suggests that this area has also been uplifted at least 3–4 m since the mid Pleistocene because of transpressional deformation along the interpreted ECFS, albeit less than that north of the river. We, therefore, refer to this area south of the Ashley River as the Clubhouse Crossroads uplift (Fig. 17a). We also considered the possibility that these outcrops are associated with buried topographic highs that were produced by differential erosion. Various observations, however, argue against this scenario. First, the incised part of the nearby Ashley River, which is interpreted to be from gentle uplift along the ECFS, crosses this area (Figs. 9, 15, profile 1, and 17a). Second, the Pleistocene fluvial deposits between the Clubhouse Crossroads area and the Edisto River (McCartan *et al.* 1984) and the continuity of the Horse Savanna Swamp with the Edisto River valley to the west (Fig. 1) suggests that the Edisto River once flowed southeastward along these swamps during the Pleistocene. Furthermore, the abrupt narrowing of the Edisto River's Holocene valley south of its intersection with the Horse Savanna Swamp (Fig. 1) and the Wando-age (70–130 ka) terraces along the edge of the lower Holocene valley (Weems *et al.* 2014) suggests that the Edisto River changed direction to the south during the late Pleistocene. We, therefore, postulate that late Pleistocene uplift across the Clubhouse Crossroads uplift and the Parkers Ferry dome (Figs. 1 and 16) diverted the Edisto River southward away from its earlier course down the Horse Savanna Swamp. Another implication of the Clubhouse Crossroads uplift is that it suggests that the ECFS continues southward beneath the Ashley River valley, rather than being offset to the southeast as previously proposed by Talwani and Durá-Gómez (2009).

The alignment of the Edisto dome, uplift along releveling line 9, and the Clubhouse Crossroads uplift (Figs. 1 and 16) with the gently upwarped longitudinal profiles along the Caw Caw and Horse Savanna swamps (Figs. 1 and 15) suggests that they are also likely from late Pleistocene to Holocene uplift along the ECFS (Figs. 1 and 16, between the red parallel lines). These upwarped profiles are not likely from differential erosion because there are no changes in the surficial geology along these swamps (Weems *et al.* 2014).

Origin of stratigraphic anomalies in the northern Charleston region

The higher terrain and anomalous exposures of the pre-Pleistocene Parkers Ferry, Ashley, Chandler Bridge, and Raysor formations in the stream valleys north of the BMS and between Four Hole Swamp to the west and the Canterhill lineament (surface expression of the Charleston fault) to the east (Figs. 16 and 17) suggest that this area has been gently uplifted during the Quaternary. Because of the more widespread pre-Pliocene outcrops along the east side of this topographically high area and because the Parkers Ferry Formation is exposed only along the east side of the ZRA (Fig. 16), we propose that the main source of this uplift is from compressional deformation along the ECFS and up-to-the-north (or down-to-the-south) displacements along the east-west-oriented McChune fault to the south (Fig. 16). The south-

Figure 17. (previous page) (a) Interpreted part of surficial geologic map of Weems *et al.* (2014) showing anomalous exposures of the pre-Pliocene Ashley and Chandler Bridge formations. Striped pattern is the ZRA. Abbreviations of faults (solid lines) and lineaments (dashed lines) are shown in Tables 1 and 2. Short-dashed pattern along the Ashley River valley shows the interpreted uplifted part of the river valley. DR, MR, and SR are the interpreted Dorchester, McChune, and Summerton ridges (thick black contours). BSW and CCU are Bluehouse Swamp and the Clubhouse Crossroads uplift. (b) Interpreted part of surficial geologic map of Weems *et al.* (2014) showing anomalous exposures of the pre-Pliocene Parkers Ferry, Ashley, and Chandler Bridge formations. Mt. Holly dome of Weems and Lewis (2002) is shown by thick black contour. The colors of the Chandler Bridge and Parkers Ferry formations were changed from Weems *et al.* (2014) to make them more visible on both maps.

dipping Cenozoic graben on seismic-reflection profile C3 (Fig. 7) suggests that the higher terrain north of this part of the BMS is from down-to-the-south displacement along the proposed McChune fault.

The alignment of the exposed Parkers Ferry sediments along tributaries of the East Branch of the Cooper River with the Bonneau dome to the southwest (Fig. 16) suggests that there may also be an area of uplift along a NE-SW-oriented buried fault. The anomalously straight Bethera paleo-barrier deposit just northwest of this trend (Fig. 16) suggests that the location of this paleo-barrier could have been influenced by uplift associated with NW-side-up displacement along this proposed buried fault.

Origin of the Cenozoic structural domes in the Charleston region

Besides uplift along Cenozoic faults, we evaluated other mechanisms to explain the interpreted Cenozoic structural domes in the Charleston region. One such mechanism is uplift along faults associated with the edges of buried Paleozoic and early Mesozoic plutons. Stevenson *et al.* (2006), for example, postulated that the edges of buried plutons in the pre-Cretaceous basement are areas of weakness where faults can form when favorably oriented relative to the direction of S_{Hmax}. However, very few of the Cenozoic domes overlie buried plutons (Fig. 16). Nor is doming of the Cenozoic strata in the Charleston region likely to fracture these uplifted strata because the deformation is too gentle. Instead, we postulate that the Cenozoic structural domes in the Charleston region are from late Cenozoic uplift along the ECFS and other buried Cenozoic faults like the Charleston fault near the southwestern edge of the Mount Holly and Mount Pleasant domes and the Ashley River fault zone beneath the Fort Bull bulge and dome (Fig. 16).

Cenozoic reactivation of a deep-seated basement fault along the ECFS

Because the ECFS crosses the Alleghanian Eastern Piedmont fault system and the early Mesozoic Florence and South Georgia rift basins, Marple and Talwani (2000) postulated that the ECFS is a Cenozoic fault system, possibly from reactivation of a pre-Alleghanian, deep-crustal fault system that was overthrust during the Alleghanian orogeny by the northwest transport of allochthonous terranes. This hypothesis is analogous to the ~1600-km-long New York-Alabama aeromagnetic lineament that is associated with a Precambrian to Cambrian right-lateral strike-slip fault system in the crystalline basement beneath the allochthonous terranes of the Allegheny Plateau and Valley and Ridge provinces (King and Zietz 1978; Steltenpohl *et al.* 2010; Powell and Thomas 2015). However, unlike the low magnetization of the terranes of the Appalachian Plateau and Valley and Ridge provinces, the higher magnetization of the allochthonous terranes beneath the thick sedimentary wedge in the Charleston region prevents detection of linear magnetic anomalies associated with pre-Mesozoic faults in the deep crust beneath the allochthonous terranes. If true, reactivation of such a deep crustal fault during Cenozoic time could have fractured through the overlying allochthonous terranes, Triassic basins, and the sedimentary wedge beneath the Coastal Plain to produce the ECFS. However, because of the low Cenozoic fault slip rate in the eastern USA (Prowell 1988, 0.3–1.5 m/myr), the accumulated strike-slip displacement along the ECFS during Cenozoic time is likely too small to be easily detected on regional gravity and aeromagnetic maps.

Summerville restraining bend

The 12° change in trend between magnetic lineaments ML5 near Summerville and ML4 to the south (Fig. 1) and their close proximity to the dextral offset in the Brownsville beach ridge deposit and buried faults along several seismic-reflection profiles (Figs. 1 and 2) support Marple and Hurd's (2020) hypothesis that the interpreted faults east of the Summerville restraining bend formed to compensate for the increased compression produced by dextral motion along the restraining bend and that displacements along the faults near the bend are responsible for the MPSSZ. Studies of fault bends have shown that secondary faults commonly develop along restraining bends in strike-slip faults (e.g., King and Nábělek 1985).

Possible relationship of the Deer Park lineament to the 1886 Charleston earthquake

The location of the Deer Park lineament in the northern meizoseismal area where the greatest intensities occurred in an east-west direction (Dutton 1889, pp. 301–302) supports our hypothesis that the main shock of the 1886 Charleston earthquake occurred along a fault associated with this lineament. The effects of the main shock in 1886 were nearly as intense near the eastern end of this area as those near Woodstock (Dutton 1889, pp. 301). Earle Sloan, for example, noted that pine trees two miles (~3.2 km) east of the Northeastern Railroad swayed violently during the main shock because dried sap had been thrown far from their trunks, the bark of which had been stripped to collect sap to make turpentine (Dutton 1889, pp. 301–302; Peters and Hermann 1986, pp. 58). Other dramatic examples of earthquake damage between Woodstock and the Cooper River are described in Dutton (1889, pp. 301–302). The Deer Park lineament also coincides approximately with the location along the old South Carolina Railroad where the direction of compressions reversed direction during the main shock in 1886 (Fig. 2, site S2, and Fig. 10), which Dutton (1889, pp. 295) emphasized in the following quote:

"Is it not a significant fact that every flexure contiguous to trestles or other points of rigid resistance, from the 15-mile post to the 27-mile post, was found to be at the south

end of such resistance; whereas preceding southerly from the 15-mile post, the flexures are found at the northerly extremities of points of resistance?"

The implication of this statement is that the main shock of the 1886 earthquake occurred on a fault that crossed the area beneath this part of the South Carolina Railroad, which we postulate is along the Deer Park lineament. The seismic waves traveling outward from the fault rupture would have produced compressional deformation in opposite directions north and south of the rupture at depth.

The alignment of the east-west-oriented part of the horseshoe-shaped Bluehouse Swamp (Fig. 17a), the "ridges or permanent waves" trending ~N80°E that Earle Sloan noted east of the old Northeastern Railroad and north of Goose Creek (Dutton 1889, pp. 291; Peters and Hermann 1986, pp. 57) (Fig. 2, site S1), the 90° eastward bend in Foster Creek (Marple and Hurd 2020, fig. 3a), and the rectangular shape of the Foster Creek depression (Marple and Hurd 2020, figs. 3a and 6a) (Fig. 17b) suggest that the proposed fault along the Deer Park lineament is associated with a broad zone of deformation and fracturing of the near surface sediments. The exposures of the Ashley Formation along the east side of the horseshoe-shaped Bluehouse and Goose Creek swamps where they cross the Deer Park lineament (Fig. 17a) suggest that uplift along the lineament exposed these older and normally buried sediments.

Possible relationship between the ECFS and Deer Park lineament and the cause of the second 1886 earthquake west of Rantowles

Studies of rupture nucleation on faults of various orientations relative to S_{Hmax} (Sibson 1990) suggest that strike-slip faults oriented 12° to 42° relative to S_{Hmax} are favorably oriented for reactivation. Thus, the 41° difference between the ~N21°E trend of the ECFS northeast of the Summerville restraining bend (ECFS(N)) and the ~N60°E orientation of S_{Hmax} (Fig. 1) favors dextral reactivation of the ECFS(N) whereas the 50° difference between this orientation of S_{Hmax} and the N10°E-oriented ECFS south of the bend (ECFS(S)) (Fig. 1) does not. However, dextral displacement along the more favorably oriented ECFS(N) would have added a south-directed horizontal stress on the crustal block east of ECFS(S) (Fig. 18). Moreover, if the direction of S_{Hmax} is closer to N50°E as proposed by Chapman *et al.* (2016), then dextral motion would also be favored on the ECFS(S).

Another mechanism that could favor dextral displacement along the ECFS(S) in 1886 is displacement on an intersecting fault, such as the interpreted fault along the Deer Park lineament. For example, the eastward motion of the crust south of the proposed Deer Park fault during the proposed sinistral-style strike-slip rupture could have decreased the normal stress on the ECFS(S) (Fig. 18), thus allowing it to slip dextrally to produce the second earthquake 8-10 minutes later west of Rantowles. An example of this mechanism is the 1987 Superstition Hills earthquake in southern California (Hudnut *et al.* 1989). During this earthquake, sinistral displacement on the NE-SW-oriented Elmore Ranch cross-fault decreased the normal stress on the NW-SE-oriented Superstitition Hills fault, thus causing it to rupture right-laterally over 11 hours later.

Conceptual model of the Summerville restraining fault bend

The interpreted deformation associated with the Summerville restraining bend is complex, as indicated by the numerous interpreted faults near the bend (Fig. 2). In general, dextral displacement across this bend would cause the area to the east to undergo compression whereas the area to the west would undergo extension (Fig. 18a). The compression to the east is accommodated by reverse and strike-slip faulting while down-to-the-south displacements along the proposed McChune fault west of the bend would accommodate extension to the west (Fig. 18a). However, this scenario changes when either the ECFS(N) or the ECFS(S) ruptures independently of the adjacent ECFS segment. For example, if only the ECFS(S) ruptures dextrally, as proposed herein in 1886, the southward movement of the crust east of ECFS(S) would favor extension, rather than compression, east of the Summerville bend (Fig. 18b), which is supported by the Cenozoic graben on seismic-reflection profile C3 that indicates normal-style faulting along the interpreted McChune fault (Fig. 7). In contrast to this scenario, the northward displacement of the crust west of the ECFS(S) would cause compression west of the Summerville bend (Fig. 18c). Other scenarios could explain the complexity of the interpreted faults associated with the Summerville bend, but are beyond the scope of this paper.

Favorable versus unfavorable orientation of faults associated with the Summerville restraining bend

Most of the interpreted faults associated with the Summerville restraining bend (Fig. 1) are favorably oriented for reactivation. The ENE-WSW orientations of the proposed faults along the Mount Holly, Middleton Place, Otranto, and Deer Park lineaments and the WNW-ESE orientation of the BMS relative to S_{Hmax} favor sinistral strike-slip displacement while the NW-SE orientations of the Charleston fault (Canterhill lineament) and the interpreted fault along the French Quarter lineament zone favor reverse-style displacement. In contrast to the ECFS and other interpreted faults east of the Summerville bend, the N57°E orientation of the Summerville fault west of the Summerville bend and other similarly oriented faults in the Charleston region are not favorably oriented for reactivation because they are nearly parallel to the N50-60°E orientation of S_{Hmax} (Fig. 1).

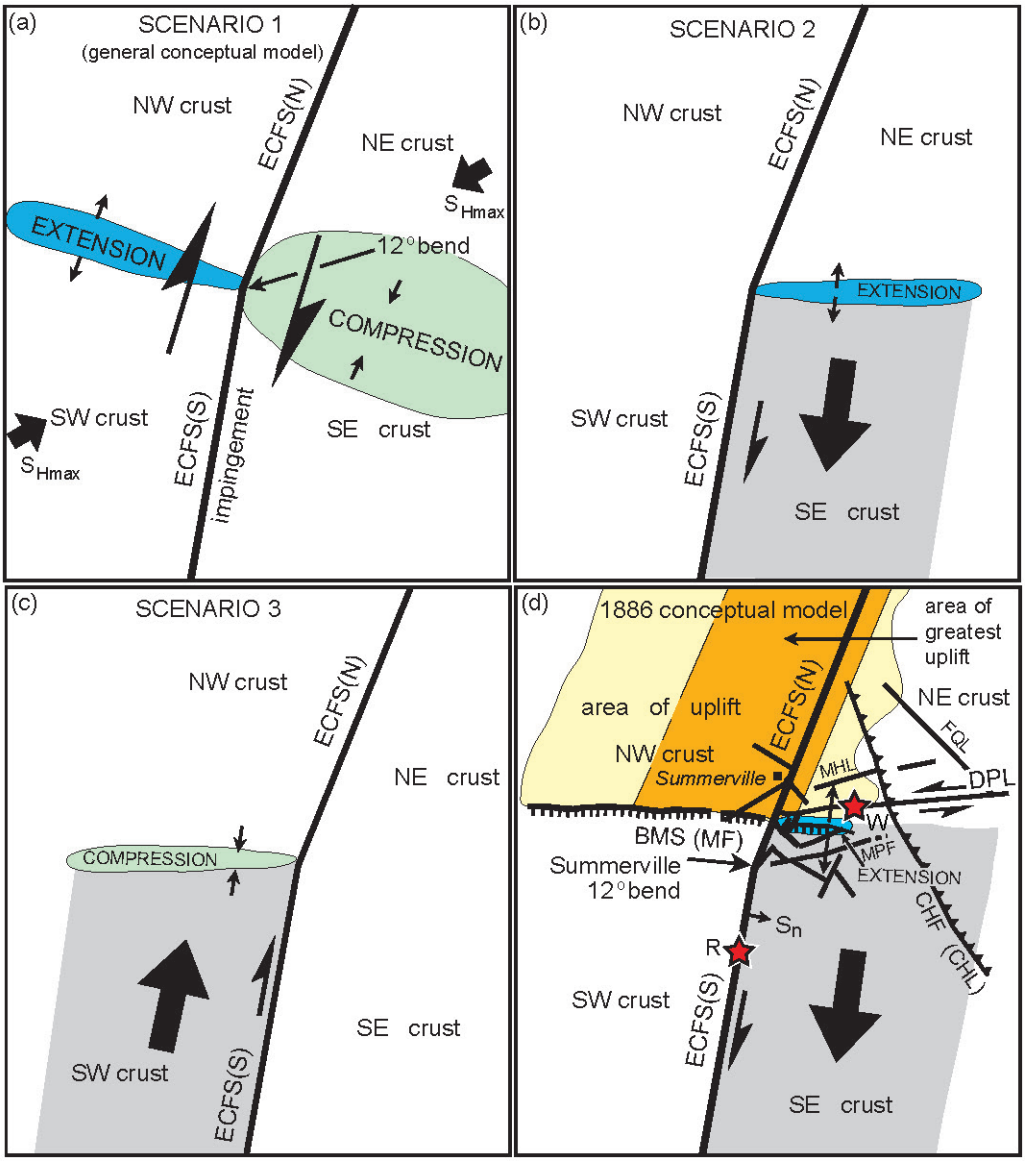

Figure 18. (a) General conceptual model showing the 12° Summerville restraining bend in the ECFS. Dextral motion along the ECFS causes compression (green pattern) east of the bend and extension (blue pattern) west of the bend. (b) Conceptual model in which the crust southeast of the restraining bend and east of the southern ECFS (ECFS(S)) moves independently of the crust east of the northern ECFS (ECFS(N)), causing extension (blue pattern) east of the Summerville bend. (c) Conceptual model in which the southwestern crust moves to the northeast, causing compression (green pattern) west of the bend. (d) Conceptual model in which sinistral motion on the Deer Park lineament (DPL) during the main shock of the 1886 Charleston earthquake decreases the normal stress (S_n) on the ECFS(S), causing it to rupture. The yellow and orange patterns to the north represent the topographically high area shown in Figures 2 and 16.

Origin and implications of the dextral offset in the Brownsville beach ridge deposit

The alignment of the dextral offset in the Pleistocene Brownsville beach ridge deposit northeast of Summerville (Fig. 8) with magnetic lineament ML5 and several buried faults interpreted from seismic-reflection profiles that cross the Summerville area (Fig. 1) strongly suggests that the beach ridge offset is from cumulative dextral strike-slip displacements along the ECFS. This offset, therefore, has several implications regarding the seismotectonics in the Charleston region. First, the ~320 m of dextral offset and the 970–730 ka age (Weems *et al.* 1997) of the Summerville barrier island complex of the Penholoway Formation yields a minimum average fault slip rate of 0.33 to 0.44 mm per year along this part of the ECFS. If, however, the Summerville barrier is part of the older Wicomico Formation (1.8–2.12 Ma, Weems *et al.* 1997) as proposed by Doar (2014), the slip rate would be smaller, 0.15–0.18 mm per year. We, therefore, postulate that the ECFS is a Cenozoic fault that has under-

gone ≤ 320 m of cumulative displacement near Summerville. Such a low amount of slip along the ECFS could explain why it is not easily identified in the landscape and on regional aeromagnetic and gravity maps of the South Carolina Coastal Plain. Another implication of the beach ridge offset relates to the orientation of S_{Hmax} in the Charleston region. Although most studies of seismicity, borehole breakouts, and GPS data suggest that the orientation of S_{Hmax} in the Charleston region is ~N50-60° E (Zoback and Zoback 1989; Madabhushi and Talwani 1993; Talwani *et al.* 1997; Chapman *et al.* 2016; Lund Snee and Zoback 2020), other recent studies (e.g., Levandowski *et al.* 2018) have suggested that S_{Hmax} is oriented nearly east-west. However, the dextral offset in the beach ridge deposit indicates that the ECFS near Summerville has undergone repeated dextral displacements since the middle Pleistocene. Thus, the direction of S_{Hmax} must be favorably oriented relative to the ~N22°E orientation of the ECFS near Summerville to cause dex-tral strike-slip displacements along the ECFS. Thus, based on Sibson's (1990) study of fault orientation relative to the horizontal compressive stress field, it is unlikely that the orientation of S_{Hmax} in the Charleston region is greater than N60°E.

The beach ridge offset also demonstrates that Cenozoic faults beneath the Coastal Plain can locally fracture the near surface sediments, albeit too minor to be easily recognized at the surface. Similarly, Marple and Hurd (2020) suggested that linear drainages along some of the LiDAR lineaments east of the Summerville restraining bend (Fig. 1) are also likely associated with minor faulting of the near surface sediments, thereby causing increased erosion and the development of linear drainages along these interpreted faults in the Charleston region.

Origin of geomorphic and stratigraphic anomalies along the Bethera-McChune scarp (BMS)

The higher elevation of the early Oligocene Ashley Formation north of the incised part of the Ashley River, the presence of the Ashley and late Oligocene Chandler Bridge formations along the south side of McChune ridge to the east (Figs. 16 and 17), and the south-dipping Cenozoic graben on seismic-reflection profile C3 (Fig. 7) suggest that the BMS is associated with north-side-up (or south-side-down) displacements along the proposed east-west-oriented Mc-Chune fault. The mid-Pleistocene Ladson barrier deposits along the tops of the Dorchester and McChune ridges (Weems *et al.* 2014, unit Qls) (Fig. 16a) suggest that north-side-up Pleistocene uplift along these ridges caused these barrier sediments to be deposited along these two ridges when sea level rose to this area 240–730 ka. Such a process was proposed by Marple *et al.* (2018) along the Merrimack ridge above the Newburyport thrust fault in northeastern Massachusetts and by Marple and Hurd (2021) along the Sloan and Jarmantown topographic highs above the interpreted Faison and Neuse faults beneath the North Carolina Coastal Plain. Thus, it is likely that the Dorchester and McChune ridges represent areas of uplift along which the Ladson barrier sediments were deposited during the mid-Pleistocene. Likewise, because the Summerwood ridge crosses various surficial sediments and because it is capped to the west by Ladson barrier sediments (Fig. 17a), it too is possibly related to Pleistocene uplift along the north side of an east-west-oriented buried fault. The alignment of the ESE-WSW-oriented tributary of Goose Creek to the southeast with the McChune Branch of Bluehouse Swamp and the anomalous exposure of late Oligocene Chandler Bridge sediments along this tributary (Fig. 17a) suggests that the proposed McChune fault continues east-southeast to the Goose Creek valley.

Origin of stratigraphic anomalies along the Ashley River fault zone

Several observations suggest that the LiDAR lineaments along the lower Ashley River represent relatively short faults of a segmented Ashley River fault zone. For example, the exposures of the Ashley Formation along the anomalously straight northeastern valley wall that defines the Ashley River lineament (ARL) and their absence along the opposite side of the valley suggests that the northeast side of this part of the valley (Fig. 17a) has been uplifted a few metres to the northeast along a fault associated with the ARL. Fracturing of the near-surface sediments near this proposed fault could have produced the fissure along the northern bank of the Ashley River valley during the 1886 earthquake shown in plate XXIII of Dutton (1889). The coincidence of the ARL with the MPSSZ suggests that this proposed fault is presently active.

Exposures of the Ashley Formation along the unnamed swamp that defines the northwestern end of the Dawkins lineament (Fig. 17a) support uplift along this lineament. Farther downstream near Middleton Gardens, the coincidence of the Dawkins lineament with outcrops of the Ashley Formation along the southwestern wall of the Ashley River valley (Fig. 16) also supports uplift along this lineament, which is consistent with the southwest-side-up fault near the southwest end of seismic-reflection profile C3 and suggests that the Dawkins lineament may be the surface expression of this fault. Exposures of the Ashley Formation and the Pleistocene terraces downstream from the Magnolia Gardens lineament (Fig. 1) and along both sides of the Ashley River valley where they cross the Fort Bull dome (Figs. 16 and 17a) suggest that this part of the valley has undergone late Quaternary uplift. The linear, northeast side of the Ashley River valley along the Lambs lineament suggests that it may be associated with uplift along a fault. Based on these observations, we postulate that Quaternary fault displacements along the Ashley River, Dawkins, Lambs, and Magnolia Gardens lineaments have produced the uplift that formed the Fort Bull dome.

Reevaluation of the ECFS

Among the most conspicuous geomorphic anomalies that define the ZRA and ECFS are the north-northeast-convex curves in the Santee, Black, and Lynches rivers in South Carolina and the Nottoway River in southeastern Virginia, which Marple and Talwani (2000) postulated were produced by a gentle, down-to-the-NNE tilt along nearby segments of the buried ECFS. Bartholomew and Rich (2012), in contrast, argued against the existence of the ECFS. Instead of a tectonic origin, they postulated that the river curves in South Carolina were produced by an early to middle Pleistocene northeastward migration of these rivers because of down-to-the-SW displacements along a NW-SE-oriented Cape Fear fault near the South Carolina/North Carolina border. Marple and Hurd (2021, pp. 317), however, argued against Bartholomew and Rich's (2012) down-to-the-NE tilt in northeastern South Carolina and the existence of the Cape Fear fault. Thus, down-to-the-NNE tilting along nearby segments of the buried ECFS remains our preferred explanation for the origin of the river curves.

Pratt *et al.* (in press) also argued against the existence of the ECFS due to the lack of conspicuous uplift along the proposed fault system. However, some seismic-reflection profiles that cross the ECFS show uplifted Cenozoic strata within a 3- to 5-km-wide zone associated with buried, up-to-the-west fault displacements (e.g., Figs. 5 and 6), although some profiles, like USC4 and USC5 (Marple and Miller 2006, figs. 12 and 13), do not show any significant vertical displacement along the trend of the ECFS. However, in these areas the predominant fault motion could be dextral strike-slip and, therefore, may not produce significant vertical offsets of the overlying strata. Moreover, the coincidence of the Edisto dome and the pre-Pliocene uplift near Summerville (Figs. 1 and 2) with the proposed ECFS shows that Oligocene strata has been gently uplifted along parts of the ECFS in the Charleston region. Pratt *et al.* (in press) also argued that the Summerville scarp (Figs. 1 and 2) should be located above the buried ECFS. This scarp, however, is a paleoshoreline scarp (e.g., Doar 2014), not a tectonic scarp. Furthermore, uplift above a steep, buried transpressional strike-slip fault like the proposed ECFS would likely produce gentle uplift of the overlying strata east and west of the fault, not just above the fault itself (e.g., Figs. 5 and 6). Lastly, several other lines of evidence support the existence of the ECFS and uplift along it, including the exposures of pre-Pleistocene strata in the northwest part of the Charleston region (Figs. 16 and 17), the uplift along releveling profile 9 (Fig. 1), the aeromagnetic lineaments presented herein (Figs. 3, 13, and 14), the dextrally offset beach ridge deposit (Fig. 8), and the local incision of the Ashley River (Figs. 1, 2, and 9).

Lack of seismicity along the ECFS

Although the orientation of the ECFS relative to the direction of S_{Hmax} favors its reactivation, recent seismicity along most of the ECFS has been low level. This observation is likely the result of the low strain rate along the Atlantic margin (10^{-9} to 10^{-10} yr^{-1}, Johnston 1989), which could cause recurrence intervals between large earthquakes along the ECFS to range from hundreds to tens of thousands of years. Numerous studies elsewhere in intraplate settings have documented evidence for Pleistocene to Holocene earthquakes along faults that currently exhibit little or no seismicity, including the Bootheel fault in southeastern Missouri (Marple and Schweig 1992; Guccione *et al.* 2005), the Saline River fault zone in southeastern Arkansas (Cox *et al.* 2012), the Newburyport fault in northeastern Massachusetts (Marple *et al.* 2018), the Faison and Neuse faults that cross the Cape Fear arch in North Carolina (Marple and Hurd 2021), the Tennant Creek earthquakes of Australia (Crone *et al.* 1997), and the proposed southwest continuation of the Norumbega fault system in southern New England where several Pleistocene drumlins are vertically offset (Marple and Hurd 2019, figs. 9 and 25).

CONCLUSIONS

In conclusion, we postulate that the NNE-SSW-oriented linear magnetic anomalies in the southern meizoseismal area of the 1886 Charleston, South Carolina, earthquake are associated with low-displacement brittle faults in the pre-Cretaceous crystalline basement and that magnetic lineaments ML4 and ML5 represent the principal displacement zone along the southern end of the ECFS. The N50-60°E orientation of S_{Hmax} relative to the ECFS in South Carolina favors its right-lateral reactivation. Evidence for Cenozoic uplift along the ECFS includes the Summerville and Clubhouse Crossroads uplifts, the zone of incision along the Ashley River, the Edisto dome near the coast, uplift along releveling profile 9, and locally upwarped longitudinal profiles along the Caw Caw and Horse Savanna swamps and along the Ashley River valley. This uplift is more pronounced north of the Ashley River.

The 12° change in trend between ML4 and ML5 supports the existence of the Summerville restraining bend along the ECFS south of the Ashley River. We postulate that the interpreted faults east of this restraining bend formed to compensate for the increased compression produced by dextral motion along the bend. We also postulate that sinistral strike-slip displacement on one of these faults associated with the ~40-km-long, east-west-oriented Deer Park lineament may have produced the main shock of the 1886 Charleston, South Carolina, earthquake. Sinistral displacement on this interpreted fault may have decreased the normal stress along the ECFS to the south, thereby causing

dextral displacement along the southern end of the ECFS and the second earthquake west of Rantowles 8–10 minutes after the main shock. Extension is generally favored west of the bend and appears to be accommodated by down-to-the-south displacements on the interpreted east-west-oriented McChune fault beneath the Bethera-McChune scarp (BMS). However, displacements along individual segments of the ECFS could have also produced local extension east of the Summerville restraining bend and compression to the west. The south-dipping Cenozoic graben east of the Summerville bend on COCORP seismic-reflection profile C3 suggests that this part of the McChune fault has undergone extension during the Cenozoic. Displacements along some of the proposed faults near the Summerville restraining bend coincide with the MPSSZ. Thus, displacements along these faults may be responsible for much of the modern seismicity between Summerville and Middleton Place. Further studies of the Summerville bend are needed, therefore, to better understand the deformation associated with this fault bend.

Exposures of the late Eocene Parkers Ferry, early Oligocene Ashley, late Oligocene Chandler Bridge, and late Pliocene Raysor formations in the stream valleys north of the proposed McChune fault and between Four Hole Swamp to the west and the Canterhill lineament (surface expression of the Charleston fault) to the east suggest that this area has been uplifted during the Quaternary with the greatest uplift between the Ashley River and Lake Moultrie. The source of this uplift is likely the result of compressional deformation along the ECFS and up-to-the-north (or down-to-the-south) displacements along the McChune fault to the south.

Several, mostly NW-SE-oriented LiDAR lineaments along the Ashley River valley south of the BMS, including the Ashley River, Dawkins, Lambs, and Magnolia Gardens lineaments, suggest that they are part of a segmented, NW-SE-oriented Ashley River fault zone. We propose that Quaternary uplift along these interpreted faults has exposed the early Oligocene Ashley Formation along various segments of the Ashley River valley and produced the Fort Bull dome and Pleistocene terraces along the lower Ashley River valley.

Further studies of the various faults interpreted herein are needed because studies of liquefaction features within the Coastal Plain of South Carolina and southeastern North Carolina have revealed several Holocene earthquakes north and south of the Charleston region (e.g., Talwani and Schaeffer 2001) where little seismicity has been recorded. These earthquakes may have occurred along the ECFS and other faults in the Coastal Plain of South Carolina and southeastern North Carolina, including the Charleston and Middleton Place faults, and the proposed McChune and Deer Park faults in the South Carolina Coastal Plain and the interpreted Neuse, Faison, and Livingston Creek faults in southeastern North Carolina (Marple andHurd 2021). Because of the rapid urbanization between Summerville and Charleston, a large earthquake today in the Charleston region would cause tremendous damage and loss of life. Therefore, further investigation of these and other potentially active faults in the Charleston region is essential to assessing seismic hazards in the southeastern United States and to better understand the evolution of Atlantic type continental margins.

ACKNOWLEDGEMENTS

We thank reviewer Ross Hartleb and Atlantic Geoscience editor Sandra Barr for their many constructive comments that helped improve our paper. This article benefited from discussions with William Doar.

REFERENCES

Bakun, W.H. and Hopper, M.G. 2004. Magnitudes and locations of the 1811–1812 New Madrid, Missouri, and the 1886 Charleston, South Carolina, earthquakes. Bulletin of the Seismological Society of America, 94, pp. 64–75. https://doi.org/10.1785/0120020122

Bartholomew, M.J. and Rich, F.J. 2007. The walls of colonial Fort Dorchester: A record of structures caused by the August 31, 1886 Charleston, South Carolina, earthquake and its subsequent earthquake history. Southeastern Geology, 44, no. 4, pp. 147–169.

Bartholomew, M.J. and Rich, F.J. 2012. Pleistocene shorelines and coastal rivers: Sensitive potential indicators of Quaternary tectonism along the Atlantic Coastal Plain of North America. *In* Recent advances in North American paleoseismology and neotectonics east of the Rockies. *Edited by* R.T. Cox, M.P. Tuttle, O.S. Boyd, and J. Locat. Geological Society of America, Special Paper 493, pp. 17–36. https://doi.org/10.1130/2012.2493(02)

Behrendt, J.C. 1983. Did movement on a northeast trending listric fault near the southeast edge of the Jedburg Triassic-Jurassic(?) basin cause the Charleston, South Carolina, 1886 earthquake? *In* A workshop on the 1886 Charleston, SC, earthquake and its implications for today. *Edited by* W.W. Hays and P.L. Gori. United States Geological Survey, Open File Report 83-843, pp. 126–131.

Bollinger, G.A. 1977. Reinterpretation of the intensity data for the 1886 Charleston, South Carolina, earthquake. *In* Studies related to the Charleston, South Carolina, earthquake of 1886: A preliminary report. *Edited by* D.W. Rankin. United States Geological Survey, Professional Paper 1028-B, pp. 17–32.

Buckner, J.C. 2011. Crustal structure in a Mesozoic extensional terrane: The South Georgia Rift and epicentral area of the 1886 Charleston, South Carolina, earthquake. Unpublished Masters thesis, Virginia Polytechnic and State University, Blacksburg, Virginia, 50 p.

Chapman, M.C. and Beale, J.N. 2008. Mesozoic and Cenozoic faulting imaged at the epicenter of the 1886 Charles-

ton, South Carolina, earthquake. Bulletin of the Seismological Society of America, 98, pp. 2533-2542. https://doi. org/10.1785/0120080923

Chapman, M.C. and Beale, J.N. 2010. On the geologic structure at the epicenter of the 1886 Charleston, South Carolina, earthquake. Bulletin of the Seismological Society of America, 100, pp. 1010–1030. https://doi.org/10.1785/0120090231

Chapman, M.C., Beale, J.N., Hardy, A.C., and Wu, Q. 2016. Modern seismicity and the fault responsible for the 1886 Charleston, South Carolina, earthquake. Bulletin of the Seismological Society of America, 106, no. 2, pp. 364–372. https://doi.org/10.1785/0120150221

Colquhoun, D.J., Woollen, I.D., Van Nieuwenhuise, D.S., Padgett, G.G., Oldham, R.W., Boylan, D.C., Howell, P.D., and Bishop, J.W. 1983. Surface and subsurface stratigraphy, structure and aquifers of the South Carolina Coastal Plain. Columbia, State of South Carolina, Office of the Governor, Ground Water Protection Division, Report for Department of Health and Environmental Control, 78 p.

Colquhoun, D.J., Johnson, G.G., Peebles, P.C., Huddlestun, P.F., and Scott, T. 1991. Quaternary geology of the Atlantic Coastal Plain. *In* Quaternary nonglacial geology: Conterminous U.S. Geology of North America. *Edited by* R.B. Morrison. Geological Society of America, K-2, Boulder, Colorado, pp. 629–650. https://doi.org/10.1130/DNAG-GNA-K2.629

Costain, J.K. and Glover, L., III. 1983. Seismicity in the eastern United States and the role of crustal reflectivity. *In* Proceedings of Conference XX: A workshop on "The 1886 Charleston, South Carolina, earthquake and its implications for today." *Edited by* W.G. Hays and P.L. Gori. United States Geological Survey, Open File Report 83-843, pp. 207–220.

Cox, R.T., Harris, J., Forman, S., Brezina, T., Gordon, J., Gardner, C., and Machin, S. 2012. Holocene faulting on the Saline River fault zone, Arkansas, along the Alabama-Oklahoma transform. *In* Recent advances in North American paleoseismology and neotectonics east of the Rockies. *Edited by* R.T. Cox, M.P. Tuttle, O.S. Boyd, and J. Locat. Geological Society of America, Special Paper 493, pp. 17–36. https://doi.org/10.1130/2012.2493(07)

Crone, A.J., Machette, M.N., and Bowman, J.R. 1997. Episodic nature of earthquake activity in stable continental regions revealed by palaeoseismicity studies of Australian and North American Quaternary faults. Australian Journal of Earth Sciences, 44, pp. 203–214. https://doi.org/10.1080/08120099708728304

Daniels, D.L. 2005. South Carolina aeromagnetic and gravity maps and data: A website for the distribution of data. United States Geological Survey, Open File Report 2005-1022. https://doi.org/10.3133/ofr20051022, accessed 1 March 2020.

Daniels, D.L., Zietz, I., and Popenoe, P. 1983. Distribution of subsurface lower Mesozoic rocks in the southeastern United States as interpreted from regional aeromagnetic and gravity maps. *In* Studies related to the Charleston, South Carolina, earthquake of 1886–Tectonics and seismicity. *Edited by* G.S. Gohn. United States Geological Survey, Professional Paper 1313-K, 24 p.

Doar, W.R., III. 2014. The geologic implications of the factors that affected relative sea-level positions in South Carolina during the Pleistocene and the associated preserved high-stand deposits. Unpublished Ph.D. thesis, University of South Carolina, Columbia, South Carolina, 172 p.

Durá-Gómez, I. and Talwani, P. 2009. Finding faults in the Charleston area, South Carolina: 1. Seismological data. Seismological Research Letters, 80, pp. 883–900. https://doi.org/10.1785/gssrl.80.5.883

Dutton, C.E. 1889. The Charleston earthquake of August 31, 1886. United States Geological Survey, U.S. Government Printing Office, Washington, D.C., pp. 203–528.

Gohn, G.S. (*Editor*). 1983. Studies related to the Charleston, South Carolina, earthquake of 1886–Tectonics and seismicity. United States Geological Survey, Professional Paper 1313, 8 plates, 467 p. https://doi.org/10.3133/ofr82134

Gohn, G.S. 1988. Late Mesozoic and early Cenozoic geology of the Atlantic Coastal Plain: North Carolina to Florida. *In* The Atlantic continental margin: Geology of North America. *Edited by* R.E. Sheridan and J.A. Grow. Boulder, Colorado, Geological Society of America, I-2, pp. 107–130. https://doi.org/10.1130/DNAG-GNA-I2.107

Gohn, G.S., Houser, B.B., and Schneider, R.R. 1983. Geology of the basement rocks near Charleston, South Carolina–Data from detrital rock fragments in lower Mesozoic(?) rocks in Clubhouse Crossroads test hole #3. *In* Studies related to the Charleston, South Carolina, earthquake of 1886–Tectonics and seismicity. *Edited by* G.S. Gohn. United States Geological Survey, Professional Paper 1313-E, 22 p. https://doi.org/10.3133/ofr82134

Guccione, M., Marple, R., and Autin, W. 2005. Evidence for Holocene displacements along the Bootheel fault (lineament) in southeastern Missouri: Seismotectonic implications for the New Madrid region. Geological Society of American Bulletin, 117, no. 3/4, pp. 319–333. https://doi.org/10.1130/B25435.1

Hamilton, R.M., Behrendt, J.C., and Ackermann, H.D. 1983. Land multichannel seismic reflection evidence for tectonic features near Charleston, South Carolina. *In* Studies related to the Charleston, South Carolina, earthquake of 1886–Tectonics and seismicity. *Edited by* G.S. Gohn. United States Geological Survey, Professional Paper 1313-I, 18 p.

Hudnut, K.W., Seeber, L., and Pacheco, J. 1989. Cross-fault triggering in the November 1987 Superstition Hills earthquake sequence, southern California. Geophysical Research Letters, 16, no. 2, pp. 199–202. https://doi.org/10.1029/GL016i002p00199

Johnston, A.C. 1989. The seismicity of "stable continental interiors." *In* Earthquakes at North Atlantic passive margins: Neotectonics and postglacial rebound. *Edited by* S. Gregersen and P.W. Basham. Kluwer Academic Publishers, Dordrecht, Netherlands, NATO ASI Series C, Math-

ematical and Physical Sciences, 266, pp. 299–327. https://idoi.org/10.1007/978-94-009-2311-9_18

Johnston, A.C. 1996. Seismic moment assessment of earthquakes in stable continental regions–III, New Madrid 1811–1812, Charleston 1886 and Lisbon 1755. Geophysical Journal International, 126, pp. 314–344. https://doi.org/10.1111/j.1365-246X.1996.tb05294.x

King, E.R. and Zietz, I. 1978. The New York-Alabama lineament: Geophysical evidence for a major crustal break in the basement beneath the Appalachian basin. Geology, 6, pp. 312–318. https://doi.org/10.1130/0091-7613(1978)6<312:TNYLGE>2.0.CO;2

King, G. and Nábělek, J. 1985. Role of fault bends in the initiation and termination of earthquake rupture. Science, 228, pp. 984–987. https://doi.org/10.1126/science.228.4702.984

Lennon, G. 1985. Identification of a northwest-trending seismogenic graben near Charleston. Unpublished Masters thesis, University of South Carolina, Columbia, South Carolina, 84 p.

Levandowski, W., Herrmann, R.B., Briggs, R., Boyd, O., and Gold R. 2018. An updated stress map of the continental United States reveals heterogeneous intraplate stress. Nature Geoscience, 11, pp. 433–437. https://doi.org/10.1038/s41561-018-0120-x

Lund Snee, J. and Zoback, M.D. 2020. Multiscale variations of the crustal stress field throughout North America. Nature Communications. pp. 1–8. https://doi.org/10.1038/s41467-020-15841-5

Madabhushi, S. and Talwani, P. 1993. Fault plane solutions and relocations of recent earthquakes in Middleton Place-Summerville seismic zone near Charleston, South Carolina. Bulletin of the Seismological Society of America, 83, no. 5, pp. 1442–1466.

Markewich, H.W. 1985. Geomorphic evidence for Pliocene-Pleistocene uplift in the area of the Cape Fear arch, North Carolina. *In* Tectonic geomorphology. *Edited by* M. Morisawa and J.T. Hack. Proceedings, 15th Annual Binghamton Geomorphology Symposium. Allen and Unwin, Boston, Massachusetts, pp. 279–297.

Marple, R.T. 1994. Discovery of a possible seismogenic fault system beneath the Coastal Plain of South and North Carolina from an integration of river morphology and geological and geophysical data. Unpublished Ph.D. thesis, University of South Carolina, Columbia, South Carolina, 354 p.

Marple, R.T. 2011. Comment on the Companion articles "Finding faults in the Charleston area, South Carolina: 1. Seismological data" by I. Durá-Gómez and P. Talwani and "Finding faults in the Charleston area, South Carolina: 2. Complementary data" by P. Talwani and I. Durá-Gómez. Seismological Research Letters, 82, no. 4, pp. 599–605. https://doi.org/10.1785/gssrl.82.4.599

Marple, R.T. and Hurd, J.D., Jr. 2019. LiDAR and other evidence for the southwest continuation of and Late Quaternary reactivation of the Norumbega fault system and a cross-cutting structure near Biddeford, Maine, USA. Atlantic Geology, 55, pp. 323–359. https://doi.org/10.4138/atlgeol.2019.011

Marple, R.T. and Hurd, J.D., Jr. 2020. Interpretation of lineaments and faults near Summerville, South Carolina, USA, using LiDAR data: Implications for the cause of the 1886 Charleston, South Carolina, earthquake. Atlantic Geology, 56, pp. 73–95. https://doi.org/10.4138/atlgeol.2020.004

Marple, R.T. and Hurd, J.D., Jr. 2021. Investigation of the Cape Fear arch and East Coast fault system (ECFS) in the Coastal Plain of North Carolina and northeastern South Carolina, USA, using LiDAR data. Atlantic Geology, 57, pp. 311–341. https://doi.org/10.4138/atlgeol.2021.015

Marple, R.T. and Miller, R. 2006. Association of the 1886 Charleston, South Carolina, earthquake and seismicity near Summerville with a 12° bend in the East Coast fault system and triple-fault junctions. Southeastern Geology, 44, no. 3, pp. 101–128.

Marple, R.T. and Schweig, E.S., III. 1992. Remote sensing of alluvial terrain in a humid, tectonically active setting: "The New Marid Seismic Zone". Photogrammetric Engineering and Remote Sensing, 58, no. 2, pp. 209–219.

Marple, R.T. and Talwani, P. 1993. Evidence of possible tectonic upwarping along the South Carolina Coastal Plain from an examination of river morphology and elevation data. Geology, 21, no. 7, pp. 651–654. https://doi.org/10.1130/0091-7613(1993)021<0651:EOPTUA>2.3.CO;2

Marple, R.T. and Talwani, P. 2000. Evidence for a buried fault system in the Coastal Plain of the Carolinas and Virginia–Implications for neotectonics in the southeastern United States. Geological Society of America Bulletin, 112, no. 2, pp. 200–220. https://doi.org/10.1130/0016-7606(2000)112<200:EFABFS>2.0.CO;2

Marple, R.T., Hurd, J.D., Jr., Liu, L., Travis, S., and Altamura, R.J. 2018. Investigation of the 1727 Newbury, Massachusetts, USA, earthquake using LiDAR imagery and P-wave velocity tomography. Atlantic Geology, 54, pp. 267–283. https://doi.org/10.4138/atlgeol.2018.009

McCartan, L., Lemon, E.M., Jr., and Weems, R.E. 1984. Geologic map of the area between Charleston and Orangeburg, South Carolina. United States Geological Survey, Miscellaneous Investigations Map I-1472, 1 sheet, scale 1:250 000.

McKinley, C. 1887. A descriptive narrative of the earthquake of August 31, 1886. *In* Appendix for the City of Charleston Year Book, 1886, Walker, Evans, and Cogswell Company, Charleston, South Carolina, pp. 345–441.

Peters, K. and Herrmann, R.B. (*Editors*). 1986. First-hand observations of the Charleston earthquake of August 31, 1886, and other earthquake materials. Reports of W.J. McGee, Earle Sloan, Gabriel E. Manigault, Simon Newcomb, and others. South Carolina Geological Survey, Bulletin 41, 116 p.

Phillips, J.D. 1977. Magnetic basement near Charleston, South Carolina–A preliminary report. *In* Studies related

to the Charleston, South Carolina, earthquake of 1886–A preliminary report. *Edited by* D.W. Rankin. United States Geological Survey, Bulletin 1028-J, 11 p.

Phillips, J.D. 1988. Buried structures at the northern end of the early Mesozoic South Georgia Basin, South Carolina, as interpreted from aeromagnetic data. *In* Studies of the early Mesozoic basins of the eastern United States. *Edited by* A.J. Froelick and G.R. Robinson. United States Geological Survey, Bulletin 1776, pp. 248–252.

Poley, C.M. and Talwani, P. 1986. Recent vertical crustal movements near Charleston, South Carolina. Journal of Geophysical Research, 91, pp. 9056–9066. https://doi.org/10.1029/JB091iB09p09056

Popenoe, P. and Zietz, I. 1977. The nature of the geophysical basement beneath the Coastal Plain of South Carolina and northeastern Georgia. *In* Studies related to the Charleston, South Carolina, earthquake of 1886–A preliminary report. *Edited by* D.W. Rankin. United States Geological Survey, Bulletin 1028-I, 19 p.

Powell, C.A. and Thomas, W.A. 2015. Grenville basement structure associated with the Eastern Tennessee seismic zone, southeastern USA. Geology, 44, no. 1, pp. 39–42. https://doi.org/10.1130/G37269.1

Pratt, T.L., Shah, A.K., Counts, R.C., Horton, J.W., Jr., and Chapman, M.C. in press. Shallow faulting and folding in the epicentral area of the 1886 Charleston, South Carolina, earthquake. Bulletin of the Seismological Society of America, 27 p. https://doi.org/10.1785/0120210329

Prowell, D.C. 1988. Cretaceous and Cenozoic tectonism on the Atlantic coastal margin. *In* The Atlantic continental margin: Geology of North America. *Edited by* R.E. Sheridan and J.A. Grow. Boulder, Colorado, Geological Society of America, I-2, pp. 557–564. https://doi.org/10.1130/DNAG-GNA-I2.557

Rankin, D.W. (*Editor*). 1977. Studies related to the Charleston, South Carolina, earthquake of 1886–A preliminary report. United States Geological Survey, Bulletin 1028, 204 p. https://doi.org/10.3133/pp1028

Rhea, S. 1989. Evidence of uplift near Charleston, South Carolina. Geology, 17, pp. 311–315. https://doi.org/10.1130/0091-7613(1989)017<0311:EOUNCS>2.3.CO;2

Schilt, F.S., Brown, L.D., Oliver, J.E., and Kaufman, S. 1983. Surface structure near Charleston, South Carolina: Results of COCORP reflection profiling in the Atlantic Coastal Plain. *In* Studies related to the Charleston, South Carolina, earthquake of 1886–Tectonics and seismicity. *Edited by* G.S. Gohn. United States Geological Survey, Professional Paper 1313-H, 19 p.

Schumm, S.A. 1986. Alluvial river response to active tectonics. *In* Studies in Geophysics: Active Tectonics. National Academy Press, Washington, D.C., pp. 80–94.

Seeber, L. and Armbruster, J.G. 1981. The 1886 Charleston, South Carolina earthquake and the Appalachian detachment. Journal of Geophysical Research, 86, no. B9, pp. 7874–7894. https://doi.org/10.1029/JB086iB09p07874

Shedlock, K.M. 1988. Seismicity in South Carolina. Seismological Research Letters, 59, pp. 165–171. https://doi.org/10.1029/JB086iB09p07874

Sibson, R.H. 1990. Rupture nucleation on unfavorably oriented faults. Bulletin of the Seismological Society of America, 80, pp. 1580–1604.

Sims, P.K. 2009. The Trans-Rocky Mountain fault system–A fundamental Precambrian strike-slip system. United States Geological Survey, Circular 1334, 13 p. https://doi.org/10.3133/cir1334

Soller, D.R. 1988. Geology and tectonic history of the lower Cape Fear River valley, southeastern North Carolina. United States Geological Survey, Professional Paper 1466-A, 60 p. https://doi.org/10.3133/pp1466A

Stein, R.S. and Yeats, R.S. 1989. Hidden earthquakes. Scientific American, 260, no. 6, pp. 48–57. https://doi.org/10.1038/scientificamerican0689-48

Steltenpohl, M.G., Zietz, I., Horton, J.W., Jr., and Daniels, D.L. 2010. New York-Alabama lineament: A right-slip fault bordering the Appalachians and mid-continent North America. Geology, 38, no. 6, pp. 571–574. https://doi.org/10.1130/G30978.1

Stevenson, D., Gangopadhyay, A., and Talwani, P. 2006. Booming plutons: Source of microearthquakes in South Carolina. Geophysical Research Letters, 33, 4 p. https://doi.org/10.1029/2005GL024679

Talwani, P. 1982. An internally consistent pattern of seismicity near Charleston, South Carolina. Geology, 10, pp. 655–658. https://doi.org/10.1130/0091-7613(1982)10%3C654:ICPOSN%3E2.0.CO;2

Talwani, P. 1999. Fault geometry and earthquakes in continental interiors. Tectonophysics, 305, pp. 371–379. https://doi.org/10.1016/S0040-1951(99)00024-4

Talwani, P. and Durá-Gómez, I. 2009. Finding faults in the Charleston area, South Carolina: 2. Complementary data. Seismological Research Letters, 80, pp. 901–919. https://doi.org/10.1785/gssrl.80.5.901

Talwani, P. and Schaeffer, W.T. 2001. Recurrence rates of large earthquakes in the South Carolina Coastal Plain based on paleoliquefaction data. Journal of Geophysical Research, 106, pp. 6621-6642. https://doi.org/10.1029/2000JB900398

Talwani, P., Kellog, J.N., and Trenkamp, R. 1997. Validation of tectonic models for an intraplate seismic zone, Charleston, South Carolina, with GPS geodetic data. United States Nuclear Regulatory Commission, Report no. NUREG CR-6529, United States Nuclear Regulatory Commission. Washington, D.C., 41 p. https://doi.org/10.2172/446309

U.S. Geological Survey. 2021. Earthquakes map. https://earthquake.usgs.gov/earthquakes/map/?extent=32.9198,-80.19642&extent=32.97044,-80.09617&range=search&baseLayer=terrain&timeZone=utc&search=%7B%22name%22:%22Search%20Results%22,%22params%22:%7B%22starttime%22:%221900-01-01%2000:00:00%22,%22maxlatitude%22:35.317,%22minlatitude%22:31.85,%22maxlongitude%22:-78.459,%22minlongitude%22:-83.513,%22minmagnitude%22:0,%22orderby%22:%22time%22%7D%7D

Weems, R.E. and Lemon, E.M., Jr. 1984. Geologic map of the Mount Holly Quadrangle, Berkeley and Charleston counties, South Carolina. United States Geological Survey, Geologic Quadrangle Map GQ-1579, 1 sheet, scale 1:24 000.

Weems, R.E. and Lemon, E.M., Jr. 1988. Geologic map of the Ladson Quadrangle, Berkeley, Charleston, and Dorchester counties, South Carolina. United States Geological Survey, Miscellaneous Investigations Map GQ-1630, 1 sheet, scale 1:24 000.

Weems, R.E. and Lewis, W.C. 2002. Structural and tectonic setting of the Charleston, South Carolina, region: Evidence from the Tertiary stratigraphic record. Geological Society of America Bulletin, 114, pp. 24–42. https://doi.org/10.1130/0016-7606(2002)114<0024:SATSOT>2.0.CO;2

Weems, R.E. and Obermeier, S.F. 1989. The 1886 Charleston earthquake–An overview of geological studies. *In* Proceedings of the United States Nuclear Regulatory Commission, Seventeenth Water Reactor Safety Information Meeting, United States Nuclear Regulatory Commission, Report no. NUREG/CP-0105, 2, Rockville, Maryland, pp. 289–313.

Weems, R.E., Lemon, E.M., Jr., and Nelson, M.S. 1997. Geology of the Pringleton, Ridgeville, Summerville, and Summerville Northwest 7.5-minute quadrangles, Berkeley, Charleston, and Dorchester counties, South Carolina. United States Geological Survey, Miscellaneous Investigations Series Map I-2502, 2 sheets, scale 1: 24 000.

Weems, R.E., Lewis, W.C., and Lemon, E.M., Jr. 2014. Surficial geologic map of the Charleston region, Berkeley, Charleston, Colleton, Dorchester, and Georgetown counties, South Carolina. United States Geological Survey, Open-File Report 2013-1030, 1 sheet, scale 1:100 000. https://doi.org/10.3133/ofr20131030

Wells, D.L. and Coppersmith, K.J. 1994. New empirical relationships among magnitude, rupture length, rupture width, rupture area, and surface displacement. Bulletin of the Seismological Society of America, 94, pp. 974–1002.

Yang, T., Yang, X., Duan, Q., Chen, J., and Dekkers, M.J. 2016. Rock magnetic expression of fluid infiltration in the Yingxiu-Beichuan fault (Longmen Shan thrust belt, China). Geochemistry, Geophysics, Geosystems, 17, pp. 1065–1085. https://doi.org/10.1002/2015GC006095

Zoback, M.D. and Zoback, M.L. 1989. Tectonic stress field of the continental United States. Geological Society of America, Memoir 172, pp. 523–540. https://doi.org/10.1130/MEM172-p523

Editorial responsibility: Sandra M. Barr